Theoretical investigation of the dependence of double beta decay tracks in a Ge detector on particle and nuclear physics parameters and separation from gamma ray events

H. V. Klapdor-Kleingrothaus*
Max-Planck-Institut für Kernphysik, Postfach 103980, D-69029, Heidelberg, Germany

I. V. Krivosheina†
Max-Planck-Institut für Kernphysik, Postfach 103980, D-69029, Heidelberg, Germany

I. V. Titkova‡
Laboratory of Nuclear Problems, Joint Institute for Nuclear Research, 141980 Dubna, Russia
(Received 2 September 2005; published 25 January 2006)

The sizes of tracks of events of neutrinoless double-beta decay in a Germanium detector depend on particle physics and nuclear physics parameters such as neutrino mass, right-handed current parameters, etc., and nuclear matrix elements. In this paper for the first time Monte Carlo simulations of neutrino-accompanied ($2\nu\beta\beta$) and neutrinoless double-beta decay ($0\nu\beta\beta$) events, and of various kinds of background processes such as multiple and other γ interactions are reported for a Ge detector. The time history of the evolution of the individual events is followed and the sizes of the events (partial volumes in the detector inside which the energy of the event is released) are investigated. Effects of the angular correlations of the two electrons in $\beta\beta$ decay, which again depend on the above nuclear and (for $0\nu\beta\beta$ decay) on particle physics parameters, are taken into account and have been calculated for this purpose for the first time on basis of the experimental half-life of ^{76}Ge and of realistic nuclear matrix elements. The sizes determine, *together* with the location of the events in the detector, the pulse shapes to be observed. It is shown for $\beta\beta$ decay of ^{76}Ge, that $\beta\beta$ events should be selectable with high efficiency by rejecting large size (high multiplicity) γ events. Double-escape peaks of similar energy of γ lines show concerning their sizes similar behavior as $0\nu\beta\beta$ events, and in that sense can be of some use for corresponding 'calibration' of pulse shapes of the detector. The possibility to distinguish $\beta\beta$ events from γ events is found to be essentially independent of the particle physics parameters of the $0\nu\beta\beta$ process. A brief outlook is given on the potential of future experiments with respect to determination of the particle physics parameters $\langle m_\nu \rangle, \langle \lambda \rangle, \langle \eta \rangle$.

DOI: 10.1103/PhysRevD.73.013010 PACS numbers: 14.60.Pq, 23.40.-s, 29.40.-n, 95.55.Vj

I. INTRODUCTION

The question whether neutrinos are massive or massless has become one of the most important topics of particle physics and astrophysics. For massive neutrinos there arises the even more fundamental question whether they are Dirac or Majorana particles. In *models* like SO(10), and most other GUT models, neutrinos *are* Majorana particles. The $\beta\beta$ decay is probably the only process which can decide directly the Dirac or Majorana nature of the neutrinos. The main two decay modes are: the neutrino-accompanied-mode ($2\nu\beta\beta$), allowed in the standard model,

$$N_A(A, Z) \rightarrow N_B(A, Z + 2) + 2e^- + 2\tilde{\nu}_e, \qquad (1)$$

and the neutrinoless mode ($0\nu\beta\beta$), which cannot occur in the standard model, since it violates total lepton number by $\Delta L = 2$,

$$N_A(A, Z) \rightarrow N_B(A, Z + 2) + 2e^-. \qquad (2)$$

The $0\nu\beta\beta$ mode can occur only when neutrinos are Majorana particles and have a nonvanishing mass (see, e.g. [1–3]).

The most sensitive experiment over the last 13 years already, is the HEIDELBERG-MOSCOW experiment [4] using High Purity Ge detectors enriched in the double-beta emitter ^{76}Ge to 86%. From this experiment evidence has been reported for this decay mode on a 4.2σ level [5–12].

The first proof for observation of this rare process in a $\beta\beta$ experiment is *to find a line at the right energy*—$Q_{\beta\beta}$. A *further* proof is to show that this line is mostly consisting of e^-e^- events and *not* of γ events, to rule out that one just has found a new γ-line [5,6]. For this proof one has to discriminate single-site events (SSE) against multiple-site events (MSE) in the germanium crystal. Double-beta events are overwhelmingly SSE, i.e, events confined to a few mm region in the detector. SSE can *also* be produced by γ-rays in *single*-Compton scattering, photoelectric interactions, or multiple-site interactions within a small distinct region. Therefore, the background of γ rays in a

*Electronic address: H.Klapdor@mpi-hd.mpg.de
Spokesman of HEIDELBERG-MOSCOW (and GENIUS-TF) Collaboration.
Homepage: http://www.mpi-hd.mpg.de.non_acc/
†Electronic address: Irina.Krivosheina@mpi-hd.mpg.de
On leave from Radiophysical-Research Institute, Nishnii-Novgorod, Russia.
‡Electronic address: kitti@nusun.jinr.ru
On leave from JINR, Dubna, Russia.

measured spectrum of $\beta\beta$ decay has to be kept extraordinarily low. MSE result from multiple-Compton scattering, and single-Compton scattering plus photoelectric absorption of photons taking place at some distance from the single-Compton scattering.

The discrimination of SSE and MSE events seems to be one of the *keys to* prove the existence of neutrinoless $\beta\beta$ decay, since experiments looking for the *tracks* of the electrons are not feasible like EXO using liquid xenon [13], or not sensitive enough like (Super-) NEMO [14] (see [11] for some discussion). Further these experiments have rather bad energy resolution. Other experiments like CUORICINO/CUORE [15] have *in general* unfortunately no way to distinguish between β and γ events, however they may benefit from detector modularity which should allow rejection of some fraction of the Compton gamma-ray background.

In this paper we present for the first time a systematic Monte Carlo investigation of the sizes of events in Ge detectors (i.e. the partial volume in the detector, in which the energy is released) for double-beta events (2ν and 0ν processes) including effects of the angular correlations of the two emitted electrons which again depend on particle physics (for $0\nu\beta\beta$) and nuclear structure parameters of these processes, and also of various types of γ-events. The knowledge of the distribution of sizes of events is of central importance for a later calculation of the pulse shapes produced by the events in the detectors, and subsequent pulse shape analysis of measured $\beta\beta$ spectra, aiming at discrimination of $\beta\beta$ and γ events and determination of the spatial locations of individual events in the detectors, which can be done by appling neuronal methods or other methods [5,6,16–18].

The used formulas, and results obtained for the spectral-angular distributions for the neutrino-accompanied and neutrinoless $\beta\beta$ decay are given in Sec. II. In Sec. III the results of Monte Carlo simulations of event sizes are given for $\beta\beta$ events, γ-Compton-scattering, single-escape events, double-escape events, and events with full energy, deposited in the detector. Some conclusions are presented in Sec. IV.

II. SPECTRAL-ANGULAR CORRELATIONS FOR THE $2\nu\beta\beta$ AND $0\nu\beta\beta$ DECAY FOR THE $0^+ \rightarrow 0^+$ TRANSITION

A. $2\nu\beta\beta$ Decay

1. Formalism

The main assumptions and approximations used for the $\beta\beta$ decay are as follows [19]:

(1) The nonrelativistic impulse approximation is used for the hadronic current.
(2) Only nonvanishing leading contributions to the decay amplitudes are retained. That is, the S-wave is used for all leptons, and only first terms of the power series expansion of the radial wave function are kept. The recoil effect of nucleons is neglected.
(3) Masses of neutrinos are neglected in calculating the phase-space integral in the final states.
(4) The recoil energy of the daughter nucleus is neglected because it is of the order of 0.1 keV at most.

In the $0^+ \rightarrow 0^+$ transition the emitted electrons are in the S-wave state and P-wave state with j = 1/2. The half-life of the $0^+ \rightarrow 0^+$ transition in the $\beta\beta$ mode is expressed as [1,19–22]

$$[T_{2\nu}(0^+ \rightarrow 0^+)]^{-1} = \left| \frac{M^{2\nu}_{GT}}{\mu_0} \right|^2 G_{GT}, \tag{3}$$

where $M^{2\nu}_{GT}$ is the nuclear matrix element, and G_{GT} is the phase-space factor:

$$G_{GT} = g_0 \int d\Omega_{2\nu} a(\epsilon_1\epsilon_2)[\langle\mu_a\rangle(\langle K_a\rangle + \langle L_a\rangle)/2]^2. \tag{4}$$

The first factor in Eq. (3) is related to the reduced nuclear matrix elements of the double Gamow-Teller (nuclear spin flip) transitions through nuclear states E_a in the intermediate nucleus by the following definition:

$$\left(\frac{M^{2\nu}_{GT}}{\mu_0}\right) = \sum_a \left(\frac{M^{2\nu}_{GTa}}{\mu_a}\right), \tag{5}$$

where $\sum_a$ means the sum over the nuclear states E_a.

$$\mu_a m_e = E_a - \frac{M_i + M_f}{2}, \tag{6}$$

m_e, M_i and M_f denote masses of electron, parent and daughter nuclei, respectively. Here the reduced nuclear matrix elements due to the double Fermi (non-spin-flip) transitions are omitted, because of their negligible contribution.

In the factor G_{GT} in Eq. (4), $g_0 = 3.78 \cdot 10^{-24} \cdot g_A^4$ yr^{-1} (we take $g_A = 1.254$), and $d\Omega_{2\nu}$ is

$$d\Omega_{2\nu} = m_e^{-11} q_1 w_1 q_2 w_2 p_1\epsilon_1 p_2\epsilon_2 \delta(\epsilon_1 + \epsilon_2 + w_1 + w_2 + M_f - M_i) dw_1 dw_2 d\epsilon_1 d\epsilon_2 dcos\theta, \tag{7}$$

where $\epsilon_k(p_k)$ and $w_k(q_k)$ are the energies (momenta) of the k-th electron and neutrino, respectively, and θ is the opening angle between the two emitted electrons. The Coulomb correction $a(\epsilon_1, \epsilon_2)$ in Eq. (4) is expressed as

$$a(\epsilon_1, \epsilon_2) = [A^2_{+1}(\epsilon_1) + A^2_{-1}(\epsilon_1)][A^2_{+1}(\epsilon_2) + A^2_{-1}(\epsilon_2)], \tag{8}$$

where $A_{\pm 1}(\epsilon)$ is the normalization of the inner Coulomb wave function and is defined as

$$A_{\pm k}(\epsilon) = [(\epsilon \pm m_e)/2\epsilon]^{1/2}[F_{k-1}(Z, \epsilon)]^{1/2} D_{\pm k}(\epsilon). \tag{9}$$

Here the first factor on the right-hand side is the normalization appearing even for the plane wave solution of the Dirac equation. The second factor $F_{k-1}(Z, \epsilon)$ is the relativistic Fermi factor, Z is the atomic number of the

daughter nucleus. This $F_{k-1}(Z, \epsilon)$ expresses the normalization of the outer regular solution for the point charge and is evaluated at the nuclear surface. The final factor $D_{\pm k}(\epsilon)$ is related with the continuity condition between the inner and outer solutions at the nuclear surface for the case of the extended nuclear charge.

The $\langle K_a \rangle$ and $\langle L_a \rangle$ in Eq. (4) come from the intermediate energy denominators due to the second-order perturbation, and are defined as

$$\langle K_a \rangle = \frac{2\langle \mu_a \rangle}{\langle \mu_a \rangle^2 - K_D^2}, \qquad \langle L_a \rangle = \frac{2\langle \mu_a \rangle}{\langle \mu_a \rangle^2 - L_D^2}, \tag{10}$$

where $\langle \mu_a \rangle$ is some average of μ_a in Eq. (5) and

$$\begin{aligned} K_D &= \frac{\epsilon_1 + w_1 - \epsilon_2 - w_2}{2m_e}, \\ L_D &= \frac{\epsilon_1 - w_1 - \epsilon_2 + w_2}{2m_e}. \end{aligned} \tag{11}$$

The replacement of μ_a by $\langle \mu_a \rangle$ means to introduce an approximation into the exact formula. The reliability of this approximation is discussed in [19] and later references. In this mode, even if a neutrino has a finite mass ($m_\nu \neq 0$), its effect is very small. Also concerning the previous assumptions, the contributions from the right-handed weak interaction are negligibly small, even if they exist and the contribution from the $P_{1/2}$ wave leptons are negligible, too.

To include explicitly the angular correlation, the transition formula is obtained by replacing $a(\epsilon_1, \epsilon_2)$ by the following combination:

$$a(\epsilon_1, \epsilon_2) - 2b(\epsilon_1, \epsilon_2)\cos\theta, \tag{12}$$

where

$$\begin{aligned} 2b(\epsilon_1, \epsilon_2) = {} & [2A_{+1}(\epsilon_1)A_{-1}(\epsilon_1)\cos(\Delta^C_{+1}(\epsilon_1) - \Delta^C_{-1}(\epsilon_1))] \\ & \times [2A_{+1}(\epsilon_2)A_{-1}(\epsilon_2) \\ & \times \cos(\Delta^C_{+1}(\epsilon_2) - \Delta^C_{-1}(\epsilon_2))], \end{aligned} \tag{13}$$

where $\Delta^C_{\pm 1}$ is an overall phase shift. The derivation and the definition of $b(\epsilon_1, \epsilon_2)$ (see Eq. (13)) are given in [20]. In order to give simpler expressions for the measurable quantities like the electron energy spectra and the angular correlation, the differential decay rate for the $0^+ \to 0^+$ transition in the $2\nu\beta\beta$ mode is re-expressed [19] in a compact form to *take out* the essential parts from $a(\epsilon_1, \epsilon_2)$ for the energy spectra and $b(\epsilon_1, \epsilon_2)$ for the angular correlation between the two emitted electrons:

$$\frac{d^3\Gamma_{2\nu}(0^+ \to 0^+)}{dT_1 dT_2 d\cos\theta} = \left| \frac{M^{2\nu}_{GT}}{\mu_0} \right|^2 N_{2\nu}[A_{2\nu}(0) + B_{2\nu}(0)\cos\theta], \tag{14}$$

where now $A_{\pm 1}(\epsilon)$ in $a(\epsilon_1, \epsilon_2)$ and $b(\epsilon_1, \epsilon_2)$ in Eqs. (8) and (13) is replaced by (9). The constant term $N_{2\nu}$ is defined by $N_{2\nu} = g_0(C_{F,0})^2$. In the nonrelativistic approximation the Fermi-factor is represented as

$$\begin{aligned} F_0(Z, \epsilon) &= \frac{2\pi\alpha Z\epsilon}{p}[1 - \exp(-2\pi\alpha Z\epsilon/p)]^{-1} \\ &= C_{F,0} \cdot d_0, \end{aligned} \tag{15}$$

where $C_{F,0}$ is the constant part of the nonrelativistic Fermi-factor, $d_0(\epsilon, p) = [1 - \exp(-2\pi\alpha Z\epsilon/p)]^{-1}$. The spectrum and angular parts in Eq. (14) are expressed by

$$\begin{aligned} \begin{pmatrix} A_{2\nu}(0) \\ B_{2\nu}(0) \end{pmatrix} = {} & (1 + T_1)^{2\gamma_1}(1 + T_2)^{2\gamma_1}(T - T_1 - T_2)^5 h_{2\nu} \\ & \times d_{00}\begin{pmatrix} A_{11} \\ -B_{11} \end{pmatrix}, \end{aligned} \tag{16}$$

where $T_j m_e = \epsilon_j - m_e$ is the kinetic energy of the j-th electron, T stands for the maximum kinetic energy release, $T m_e = M_i - M_f - 2m_e$ and $\gamma_1 = \sqrt{1 - (\alpha Z)^2}$, α is the fine structure constant. The factor $h_{2\nu}(T_1, T_2)$ related to the energy denominator is defined as

$$h_{2\nu}(T_1, T_2) = \frac{30}{4} \cdot \frac{\langle \mu_a \rangle^2}{w^5} \int_0^w dw_1 w_1^2 (w - w_1)^2 H_1, \tag{17}$$

where $w = (T - T_1 - T_2) \cdot m_e$. The constant factor comes from the normalization $\lim_{\langle \mu_a \rangle \to \infty} h_{2\nu}(T_1, T_2) = 1$. The factor H_1 is $H_1 = [\frac{\langle K_a \rangle + \langle L_a \rangle}{2}]^2$, where $\langle K_a \rangle$, $\langle L_a \rangle$ are defined in Eq. (10). In Eq. (11) K_D and L_D are expressed as

$$\begin{aligned} K_D &= [2T_1 - T + 2w_1/m_e]/2, \\ L_D &= -[2T_2 - T + 2w_1/m_e]/2. \end{aligned} \tag{18}$$

In the plane wave limit for electrons $[\alpha Z \to 0]$ the following expressions were obtained:

$$\begin{aligned} & \gamma_1 = 1, \qquad C_{F,0} = 2\pi\alpha Z, \\ & d_{00}(T_1, T_2) = (1 - e^{2\pi y_1})^{-1}(1 - e^{2\pi y_2})^{-1}, \\ & y_i = \frac{\alpha Z \epsilon_i}{p_i}, \qquad A_{11} = 1, \qquad B_{11} = \frac{p_1 p_2}{\epsilon_1 \epsilon_2}. \end{aligned} \tag{19}$$

The validity of this approximation is discussed in [20].

The final decay formula, including explicitly the angular correlation between the emitted electrons, is the following [19–21,23],

$$\frac{d^3\Gamma}{dT_1 dT_2 d\cos\theta} = A\cdot(1+T_1)^2(1+T_2)^2(T-T_1-T_2)^5 h_{2\nu}(T_1,T_2)d_0(T_1)d_0(T_2)\left[1-\frac{\sqrt{T_1T_2(T_1+2)(T_2+2)}}{(T_1+1)(T_2+1)}\cdot\cos\theta\right],$$

$$A = \left|\frac{M_{GT}}{\mu_0}\right|^2 g_0(2\pi\alpha Z)^2, \qquad d_0(T_i) = \left[1-\exp\left(-\frac{2\pi\alpha Z(T_i+1)}{\sqrt{T_i(T_i+2)}}\right)\right] \tag{20}$$

The nuclear matrix element is taken in this paper from the experimental determination of the half-life for ^{76}Ge of $T_{2\nu} = 1.74\cdot 10^{21}$ yr [24,25]. The phase-space factor was taken from [26], $G_{GT} = 1.317\times 10^{-19}$. Then the first factor in Eq. (3) is $|M^{2\nu}_{GT}/\mu_0| = 0.0661$. According to [20] for ^{76}Ge $\langle\mu_a\rangle = 18.42$.

2. Results

The calculated angular correlations for the single electron spectrum calculated for the above parameters for ^{76}Ge are presented in Fig. 1. The electrons are predominantly predicted in back-to-back directions.

B. $0\nu\beta\beta$ Decay

1. Half-life formula

The expression for the half-life is [20,21,26–28]

$$[T_{0\nu}]^{-1} = C_{mm}\left(\frac{\langle m_\nu\rangle}{m_e}\right)^2 + C_{m\lambda}\left(\frac{\langle m_\nu\rangle}{m_e}\right)\langle\lambda\rangle + C_{m\eta}\left(\frac{\langle m_\nu\rangle}{m_e}\right)\times\langle\eta\rangle + C_{\lambda\lambda}\langle\lambda\rangle^2 + C_{\eta\eta}\langle\eta\rangle^2 + C_{\lambda\eta}\langle\lambda\rangle\langle\eta\rangle, \tag{21}$$

where the C_{ij} are products of matrix elements and phase-space integrals, for the terms coming from the effective neutrino mass $\langle m\rangle = \sum_j m_j U^2_{ej}$, and from effective right-handed current parameters $\langle\eta\rangle = \eta\sum_j U_{ej}V_{ij}$ and $\langle\lambda\rangle = \lambda\sum_j U_{ej}V_{ij}$. These C_{ij} can be written as

$$\begin{aligned}
C_{mm} &= G_1(M_{GT})^2(1-\chi_F)^2,\\
C_{m\lambda} &= -(M_{GT})^2(1-\chi_F)(\chi_{2-}G_3 - \chi_{1+}G_4),\\
C_{m\eta} &= (M_{GT})^2[\chi_{2+}G_3 - \chi_{1-}G_4 - (\chi_P G_5 - \chi_R G_6)](1-\chi_F),\\
C_{\lambda\lambda} &= (M_{GT})^2\left[\chi^2_{2-}G_2 - \frac{1}{9}(2\chi_{1+}\chi_{2-}G_3 - \chi^2_{1+}G_4)\right],\\
C_{\eta\eta} &= (M_{GT})^2\left[\chi^2_{2+}G_2 - \frac{1}{9}(2\chi_{1-}\chi_{2+}G_3 - \chi^2_{1-}G_4) - \chi_P\chi_R G_7 + \chi^2_P G_8 + \chi^2_R G_9\right],\\
C_{\lambda\eta} &= -2(M_{GT})^2\left(\chi_{2+}\chi_{2-}G_2 - \frac{1}{9}[(\chi_{1+}\chi_{2+} + \chi_{1-}\chi_{2-})G_3 - \chi_{1-}\chi_{1+}G_4]\right).
\end{aligned} \tag{22}$$

In the above formulae the following combinations of the nuclear matrix elements are defined:

$$\begin{aligned}
\chi_{1\pm} &= \chi_{GTq} \pm 3\chi_{Fq} - 6\chi_T,\\
\chi_{2\pm} &= \chi_{GTW} \pm \chi_{FW} - \tfrac{1}{9}\chi_{1\pm}.
\end{aligned} \tag{23}$$

The phase-space integral can be given in the form [20–22,26]:

$$G_k = \frac{g}{r_A^2}\int_l^{T+1} b_k F_0(Z,\epsilon_1)F_0(Z,\epsilon_2)p_1p_2\epsilon_1\epsilon_2 d\epsilon_1, \tag{24}$$

with

$$\begin{aligned}
b_1 &= 1, \qquad b_2 = \frac{1}{2}\left(\frac{\epsilon_1\epsilon_2-1}{\epsilon_1\epsilon_2}\right)(\epsilon_1-\epsilon_2)^2,\\
b_3 &= \frac{(\epsilon_1-\epsilon_2)^2}{\epsilon_1\epsilon_2}, \qquad b_4 = \frac{2}{9}\left(\frac{\epsilon_1\epsilon_2-1}{\epsilon_1\epsilon_2}\right),\\
b_5 &= \frac{4}{3}\left(\frac{(T+2)\zeta}{2r_A\epsilon_1\epsilon_2} - \frac{(\epsilon_1\epsilon_2+1)}{\epsilon_1\epsilon_2}\right), \qquad b_6 = \frac{4(T+2)}{r_A\epsilon_1\epsilon_2},\\
b_7 &= \frac{16}{3}\frac{1}{r_A\epsilon_1\epsilon_2}\left(\frac{\epsilon_1\epsilon_2+1}{2r_a}\zeta - T - 2\right),\\
b_8 &= \frac{2}{9}\frac{1}{r_A^2\epsilon_1\epsilon_2}[(\epsilon_1\epsilon_2+1)(\zeta^2+4r_A^2) - 4r_A\zeta(T+2)],\\
b_9 &= \frac{8}{r_A^2}\left(\frac{\epsilon_1\epsilon_2+1}{\epsilon_1\epsilon_2}\right),
\end{aligned} \tag{25}$$

where ϵ_1, ϵ_2, p_1, p_2 are the energies and impulses of the

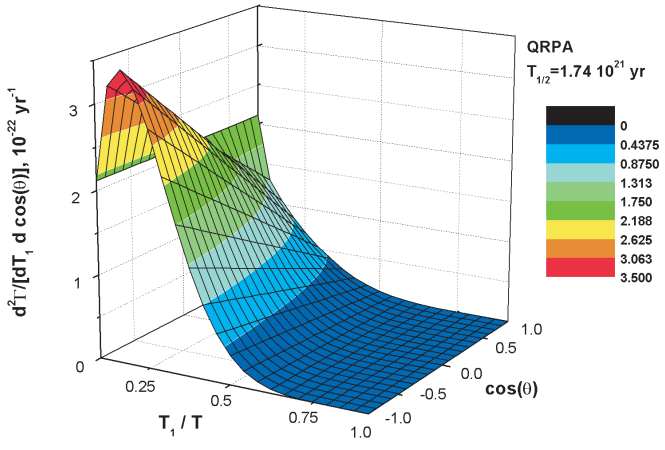

FIG. 1 (color). Calculated angular correlations of the single electron spectrum for the $0^+ \to 0^+$ transition for the $2\nu\beta\beta$ mode for ^{76}Ge.

two electrons, $r_A = m_e R_A$, $R_A = 1.2A^{1/3} fm$ and

$$\zeta = 3\alpha Z + r_A(T+2), \qquad g = 2.8 \cdot 10^{-22} g_A^4 yr^{-1}. \tag{26}$$

For the phase-space integrals we obtained:

$$\begin{aligned} G_1 &= 6.895 \cdot 10^{-15}, & G_2 &= 1.110 \cdot 10^{-14}, \\ G_3 &= 3.823 \cdot 10^{-15}, & G_4 &= 1.337 \cdot 10^{-15}, \\ G_5 &= 2.082 \cdot 10^{-13}, & G_6 &= 1.592 \cdot 10^{-12}, \\ G_7 &= 9.839 \cdot 10^{-11}, & G_8 &= 6.470 \cdot 10^{-12}, \\ & & G_9 &= 3.586 \cdot 10^{-10}. \end{aligned} \tag{27}$$

The values of the matrix elements for different nuclear models used in the calculations will be presented in Sec. II B 3.

In Eq. (21) enter contributions from a neutrino mass and from right-handed (V + A) weak interactions. The first term in Eq. (21) is proportional to the effective neutrino mass $\langle m \rangle = |\sum_j m_j U_{ej}^2|$, where the sum extends over light neutrino mass eigenstates ($m_j < 10$ MeV), and where U_{ej} are the (left-) mixing matrix elements connecting the flavor eigenstate (electron neutrino) to the mass eigenstates. This term comes from the mass part of the virtual neutrino propagator [20–22]. Since both parent and daughter nuclei have $J^p = 0^+$, it is most favorable that the two emitted electrons are in S-wave states. This situation occurs when both weak interaction vertices are of the left-handed current (V − A) type. Both emitted electrons have mainly negative helicities.

The next terms in Eq. (21) depend on the effective right-handed current parameters $\langle \eta \rangle = \eta \sum_j U_{ej} V_{ej}$, $\langle \lambda \rangle = \lambda \sum_j U_{ej} V_{ej}$. The right-handed coupling parameter λ would enter through the existence of a right-handed weak boson W_R and is determined by $\lambda = (m_{W_L}/m_{W_R})^2$, where m_{W_L} and m_{M_R} stand for the masses of the left- and right-handed weak gauge bosons, respectively. If W_L and W_R are the mixing between two mass eigenstates with masses m_{W_1} and m_{W_2}, it is possible in general to have two parameters λ and η, which are different combinations of m_{W_1} and m_{W_2} and a mixing angle ξ [29]. In this mixing scheme, if λ becomes zero, η should be zero [30]. However, it is possible to construct other scenarios, e.g, the mixing between left-handed particles and their mirror particles. In this mixing scheme there is another set of parameters η and χ. The parameter χ has no measurable contribution to the $\beta\beta$ decay, as discussed in [20]. Since the possible mixing schemes are not known, the parameters λ and η are generally treated as two independent parameters.

The three terms m_ν, λ and η in the $0\nu\beta\beta$ mode of $\beta\beta$ decay show different characteristics in the angular correlations and energy spectrum. *In principle*, knowing the single electron energy spectrum and the angular correlation of the two electrons with sufficient accuracy, one could distinguish between decays due to coupling to the left-handed and right-handed hadronic current, respectively, (see below).

If the right-handed weak interaction exists and operates at one of the electron-emitting vertices, the 4 momentum q^μ part of the virtual neutrino propagator should be taken into account. In this case the two emitted electrons have mainly opposite helicities. As for the q^μ part we meet two completely different situations, namely, the virtual neutrino energy q^0 case and the three momentum **q** case.

In the q^0 case, there is no parity-odd operator between the initial and final nuclear states. Therefore it is enough to consider only the case where the two electrons are emitted in the S-wave states. The contribution from the q^0 part is relatively suppressed, as shown, for example, in [21] for the numerical values for the decay rates due to the m_ν-term and the q^0 case.

In the **q** case one of the electrons should be in the P-wave state to satisfy the parity conservation because only the $0^+ \rightarrow 0^+$ transition is considered. Since the other electron is in the S-wave state, the P-wave electron should have a total angular momentum of one-half. In spite of the suppression due to the P-wave state, it is possible that the contribution from this **q** case is the largest in comparison with the m_ν-term and the q^0 case.

If the electron P-wave gives a large contribution, we have to consider the nucleon recoil effect, which is expressed to be of the same order of magnitude. The nucleon recoil term plays the same role as the electron P-wave (parity odd) does, so that both electrons are emitted in the S-wave state. Thus, this term may offer more dramatic contributions than the previous ones for the $\eta \neq 0$ case [19,21,31].

The half-life formula for the $0\nu\beta\beta$ mode given in Eq. (21) has been derived under the following approximations [19]:

(1) The nonrelativistic impulse approximation was used.
(2) The energy of the intermediate nuclear state E_n is replaced by the average value $\langle E_n \rangle$ and then the closure approximation is adopted.
(3) Only the first term of the electron Coulomb wave function in the expansion of r is retained (a few % error).
(4) CP conservation is assumed.

2. *Spectral-angular distribution for the* $0^+ \rightarrow 0^+$ *transition for the* $0\nu\beta\beta$ *mode*

Since the 0ν mode contains various contributions from the neutrino mass part and V + A part, the single electron kinetic energy spectrum and the angular correlations are rather complicated. The differential decay rate can be written as [19–21,23]:

$$\frac{d^3\Gamma_{0\nu}}{dT_1 dT_2 dcos\theta} = |M_{GT}|^2 N_{0\nu}[A_{0\nu}(0) + B_{0\nu}(0)cos\theta], \tag{28}$$

where the total normalization constant $N_{0\nu}$ is $N_{0\nu} = \frac{g}{(r_A)^2}(C_{F,0})^2$, θ is the angle between the two emitted electrons and

$$\begin{pmatrix} A_{0\nu}(0) \\ B_{0\nu}(0) \end{pmatrix} = (1+T_1)^{2\gamma_1}(1+T_2)^{2\gamma_1}\delta(T - T_1 - T_2) \times d_{00}\begin{pmatrix} A_{11} \\ -B_{11} \end{pmatrix}. \tag{29}$$

In the nonrelativistic approximation $A_{11} = 1$, $B_{11} = \frac{p_1 p_2}{\epsilon_1 \epsilon_2}$, and d_{00} is a Coulomb factor defined as $d_{00} = d_0(\epsilon_1, p_1) \cdot d_0(\epsilon_2, p_2)$.

Using the notation $T_2 = T - T_1$, we have the following full expression corresponding to Eq. (28) [20]:

$$\frac{d^2\Gamma_{0\nu}}{dT_1 dcos\theta} = |M_{GT}|^2 N_{0\nu}(A_{0\nu}(0) + B_{0\nu}(0)cos\theta), \qquad \begin{pmatrix} A_{0\nu}(0) \\ B_{0\nu}(0) \end{pmatrix} = (T_1+1)^{2\gamma_1}(T_2+1)^{2\gamma_1} d_{00}\begin{pmatrix} A'_0 \\ B'_0 \end{pmatrix},$$

$$A'_0 = C_1\left(\frac{\langle m_\nu\rangle}{m_e}\right)^2 + C_2\langle\lambda\rangle\frac{\langle m_\nu\rangle}{m_e}cos\Psi_1 + C_3\langle\eta\rangle\frac{\langle m_\nu\rangle}{m_e}cos\Psi_2 + C_4\langle\lambda\rangle^2 + C_5\langle\eta\rangle^2 + C_6\langle\lambda\rangle\langle\eta\rangle cos(\Psi_1 - \Psi_2),$$

$$B'_0 = \frac{p_1 p_2}{\epsilon_1\epsilon_2}\left[C'_1\left(\frac{\langle m_\nu\rangle}{m_e}\right)^2 + C'_2\langle\lambda\rangle\frac{\langle m_\nu\rangle}{m_e}cos\Psi_1 + C'_3\langle\eta\rangle\frac{\langle m_\nu\rangle}{m_e}cos\Psi_2 + C'_4\langle\lambda\rangle^2 + C'_5\langle\eta\rangle^2 + C'_6\langle\lambda\rangle\langle\eta\rangle cos(\Psi_1 - \Psi_2)\right] \tag{30}$$

In Eq. (30) Ψ_1, Ψ_2 are the CP phases. As we assumed CP conservation, $\Psi_1 = \Psi_2 = 0$ or π. The six coefficients of the spectrum part in the expression (30) are [20,26]

$$\begin{gathered} C_1 = (1-\chi_F)^2, \qquad C_2 = 2(1-\chi_F)(E_{-+}\chi_{3-} + E_{+-}\chi_{3+}), \\ C_3 = -2(1-\chi_F)(E_{-+}\chi_{4-} + E_{+-}\chi_{4+} - E_{++}\chi_{PR-} + E_{--}\chi_{PR+}), \qquad C_4 = E_{-+}\chi_{3-}^2 + E_{+-}\chi_{3+}^2, \\ C_5 = E_{-+}\chi_{4-}^2 + E_{+-}\chi_{4+}^2 + E_{++}\chi_{PR-}^2 + E_{--}\chi_{PR+}^2), \qquad C_6 = -2(E_{-+}\chi_{3-}\chi_{4-} + E_{+-}\chi_{3+}\chi_{4+}), \\ E_{+\pm} = \frac{(\epsilon_1 + m_e)(\epsilon_2 \pm m_e)}{4\epsilon_1\epsilon_2}, \qquad E_{-\pm} = \frac{(\epsilon_1 - m_e)(\epsilon_2 \pm m_e)}{4\epsilon_1\epsilon_2}. \end{gathered} \tag{31}$$

In these equations the following combinations of the nuclear matrix elements are used:

$$\chi_{3\pm} = \frac{2}{9}\chi_{1+} \pm \frac{\epsilon_1 - \epsilon_2}{m_e}\chi_{2-}, \qquad \chi_{4\pm} = \frac{2}{9}\chi_{1-} \pm \frac{\epsilon_1 - \epsilon_2}{m_e}\chi_{2+}, \qquad \chi_{PR\pm} = \frac{4}{r_A}\left[\chi_R - \frac{1}{6}(\zeta \pm 2r_A)\chi_P\right] \tag{32}$$

The value of ζ is defined by (26), all nuclear parameters are defined in [20] and assumed to be real.

Similarly, the six coefficients for the angular part of expression (30) are [20]

$$\begin{gathered} C'_1 = -(1-\chi_F)^2\frac{\epsilon_1\epsilon_2}{p_1 p_2}, \qquad C'_2 = -(1-\chi_F)\frac{2}{9}\chi_{1+}, \qquad C'_3 = (1-\chi_F)\left(\frac{2}{9}\chi_{1-} - \frac{4}{3}\chi_P + E_{--}\chi_{PR+}\right), \\ C'_4 = \frac{1}{2}\left[\left(\frac{\epsilon_1 - \epsilon_2}{m_e}\chi_{2-}\right)^2 - \left(\frac{2}{9}\chi_{1+}\right)^2\right], \qquad \left(C'_5 = \frac{1}{2}\left[\left(\frac{\epsilon_1 - \epsilon_2}{m_e}\chi_{2+}\right)^2 - \left(\frac{2}{9}\chi_{1-}\right)^2\right] + \left[\frac{8}{r_A^2}\left(\frac{1}{6}\zeta\chi_P - \chi_R\right)^2 - \frac{8}{9}\chi_P^2\right], \\ C'_6 = -\left[\left(\frac{\epsilon_1 - \epsilon_2}{m_e}\chi_{2-}\right)\left(\frac{\epsilon_1 - \epsilon_2}{m_e}\chi_{2+}\right) - \left(\frac{2}{9}\chi_{1-}\right)\left(\frac{2}{9}\chi_{1+}\right)\right]. \end{gathered} \tag{33}$$

The expressions for $\chi_1\pm$, $\chi_2\pm$ are given by Eq. (23).

Some discussion of the *general* shapes of the spectra and angular correlations for the $\langle m_\nu\rangle^2, \langle\lambda\rangle^2, \langle\eta\rangle^2$ parts in expression (30) is already given, for example, in [20,21,23,30]. In the next subsection we investigate in detail the case of ^{76}Ge decay exploiting *the present knowledge of the experimental half-life and using realistic matrix elements*.

TABLE I. Nuclear matrix elements of the neutrinoless double-beta decay of ^{76}Ge calculated with different nuclear models and effective interactions. Here $\chi_\alpha = \frac{M_\alpha}{M_{GT}}$.

Model	M_{GT}	χ_F	χ_{GTW}	χ_{FW}	χ_{GTq}	χ_{Fq}	χ_T	χ_P	χ_R
QRPA[28]	3.01	−0.39	0.97	−0.34	0.65	−0.35	−0.20	−0.18	1.19
SM[33]	4.17	−0.20	1.00	−0.20	1.14	−0.23	−0.01	0.27	0
VAMPIR[31]	5.72	−0.22	0.86	−0.18	1.14	−0.26	−0.03	−0.22	0.42

3. *Spectral-angular distributions for the* $0\nu\beta\beta$ *decay of* ^{76}Ge

The angular correlations of the electrons in $0\nu\beta\beta$ decay of ^{76}Ge required for the Monte Carlo calculation of the tracks in the detector are calculated here using the values of the matrix elements from the proton-neutron quasiparticle random phase approximation (QRPA) [28,32], which should give a realistic description. For demonstration of the sensitivity of the calculated angular correlations to the chosen nuclear model also calculations for the very simple shell model (SM) [33], and for the VAMPIR approach [31] are given.

The QRPA calculation [28,32] yielded the best *prediction* of the matrix element of $2\nu\beta\beta$ decay of ^{76}Ge *which was not yet measured at the time of that calculation* (deviation from the later experiment [24,25] only 29%). The shell model is known to have general problems to describe the large configuration space of a heavy nucleus such as ^{76}Ge (see [1,27]).

The nine matrix elements required for the calculations are shown for each of these models in Table I.

For the calculations of the effective mass $\langle m_\nu \rangle$, and the parameters of the right-handed current contributions $\langle \lambda \rangle$ and $\langle \eta \rangle$, and finally the spectral-angular distributions the experimental value of the half-life was used: $T_{1/2} = 1.19 \cdot 10^{25}$ years [5,6].

Spectral-Angular Distribution for QRPA: According to Table I in the frame of the QRPA approach from [28] we find the constraints on the effective neutrino mass and on the two parameters of the right-handed current contributions shown in Fig. 2. The insides of the ellipsoids are the allowed domains (assuming *CP* conservation). Under the purely phenomenological condition that only one of the terms contributes (this assumption is often made in analysis of $\beta\beta$ experiments), we find,

$$\begin{aligned} &\langle m_\nu \rangle = 0.4264 \text{ eV}, \quad \langle \lambda \rangle = 0, \quad \langle \eta \rangle = 0; \\ &\langle m_\nu \rangle = 0 \text{ eV}, \quad \langle \lambda \rangle = 9.509 \cdot 10^{-7}, \quad \langle \eta \rangle = 0; \\ &\langle m_\nu \rangle = 0 \text{ eV}, \quad \langle \lambda \rangle = 0, \quad \langle \eta \rangle = 4.187 \cdot 10^{-9}. \end{aligned} \tag{34}$$

In the frame of Grand Unified Models the terms are *not* independent, and a right-handed current contribution can occur *only*, when the neutrino has a *finite* (Majorana) mass (see [1,3,34]).

The maximum value of $\langle m_\nu \rangle$ is obtained to be (see Fig. 2)

$$\begin{aligned} &\langle m_\nu \rangle = 0.5028 \text{ eV}, \quad \text{with} \quad \langle \lambda \rangle = 1.793 \cdot 10^{-7}, \\ &\langle \eta \rangle = -2.495 \cdot 10^{-9}. \end{aligned} \tag{35}$$

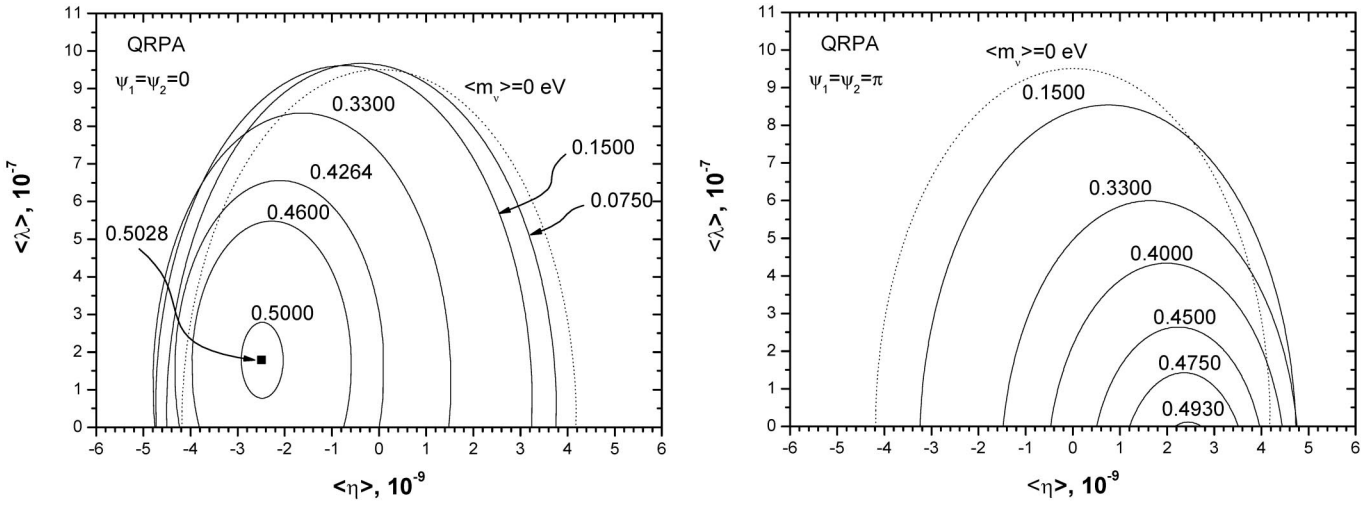

FIG. 2. Allowed parameters for $\langle m_\nu \rangle$, $\langle \lambda \rangle$, $\langle \eta \rangle$ from the measured half-life of $0\nu\beta\beta$ decay of ^{76}Ge [5,6] according to analysis with QRPA [28] from Table I (*CP* parities $\psi_1 = \psi_2 = 0$ (left) and $\psi_1 = \psi_2 = \pi$ (right)).

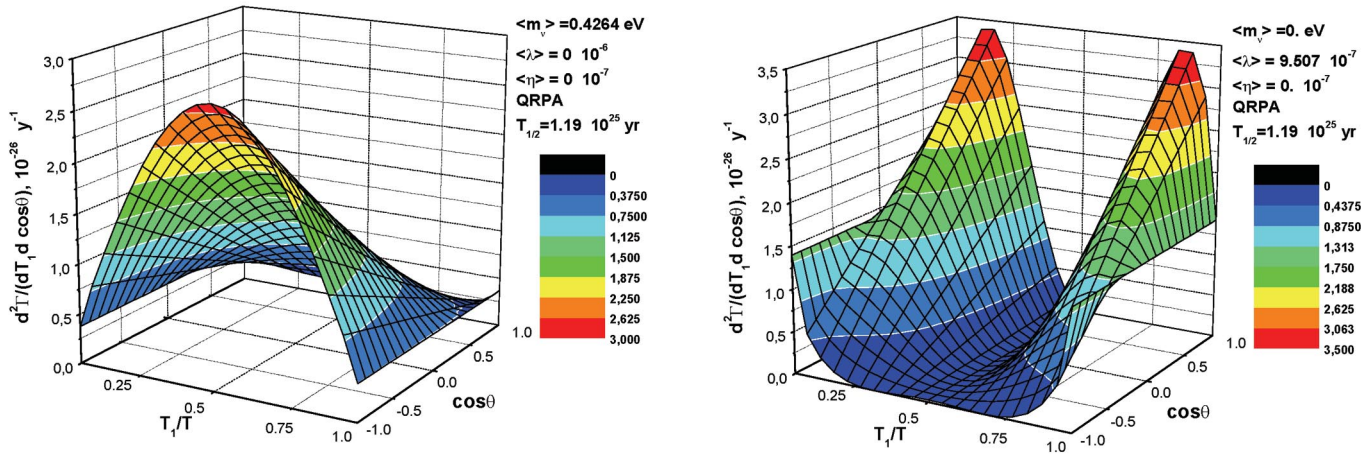

FIG. 3 (color). Calculated spectral-angular correlation for the neutrino mass term for $0\nu\beta\beta$ decay of ^{76}Ge (left), and for the $\langle\lambda\rangle^2$-term (right) (QRPA from [28]).

The corresponding values for the half-lives $T^{0\nu}_{1/2} = 0.69$ and $4.18 \cdot 10^{25}$ yr (3σ allowed range according to [5]) are

$$\begin{aligned} &\langle m_\nu\rangle = 0.66 \text{ eV}, \quad &&\langle\lambda\rangle = 2.36 \cdot 10^{-7}, \quad &&\langle\eta\rangle = -3.28 \cdot 10^{-9}, \\ &\langle m_\nu\rangle = 0.23 \text{ eV}, \quad &&\langle\lambda\rangle = 9.59 \cdot 10^{-8}, \quad &&\langle\eta\rangle = -1.33 \cdot 10^{-9}. \end{aligned} \tag{36}$$

The values for $\langle m\rangle$ could be somewhat, up to ~30%, *lower* then deduced above, when considering that the $0\nu\beta\beta$ matrix element may be slightly *underestimated*, as the $2\nu\beta\beta$ matrix element (see above). As obvious from Fig. 2, the experiment gives *very sharp limits* for the right-handed current contributions η, λ *in addition* to the effective neutrino mass.

The spectral-angular distributions for the sets of parameters Eqs. (34) and (35) are shown in Figs. 3 and 4.

When *only* the neutrino mass term is considered, both electrons are emitted from a V − A vertex, so that their main helicities are the same. Because of the angular momentum conservation in the plane made of two electrons, two S-wave electrons should be emitted predominantly in the *back-to-back* configuration for the $0^+ \to 0^+$ transition (Fig. 3 left). For the V + A part, one electron is emitted from the V − A vertex and the other is from the V + A vertex, and thus their main helicities are opposite. Therefore, two electrons with $j = 1/2$ are emitted mostly in the same directions (Figs. 3—right and 4—left). When all three parameters are nonzero the situation may be different. For a "large" neutrino mass the mass term plays the main role, the electrons are emitted in opposite directions (Fig. 4—right). But, for example, for the values $\langle m_\nu\rangle = 0.33$ eV, $\langle\lambda\rangle = 4.953 \cdot 10^{-7}$, $\langle\eta\rangle = 0$, which are also consistent with the experiment (see Fig. 2), the role of the mass term and the roles of right-handed parameters are approximately equal (Fig. 5). In this case the electrons can

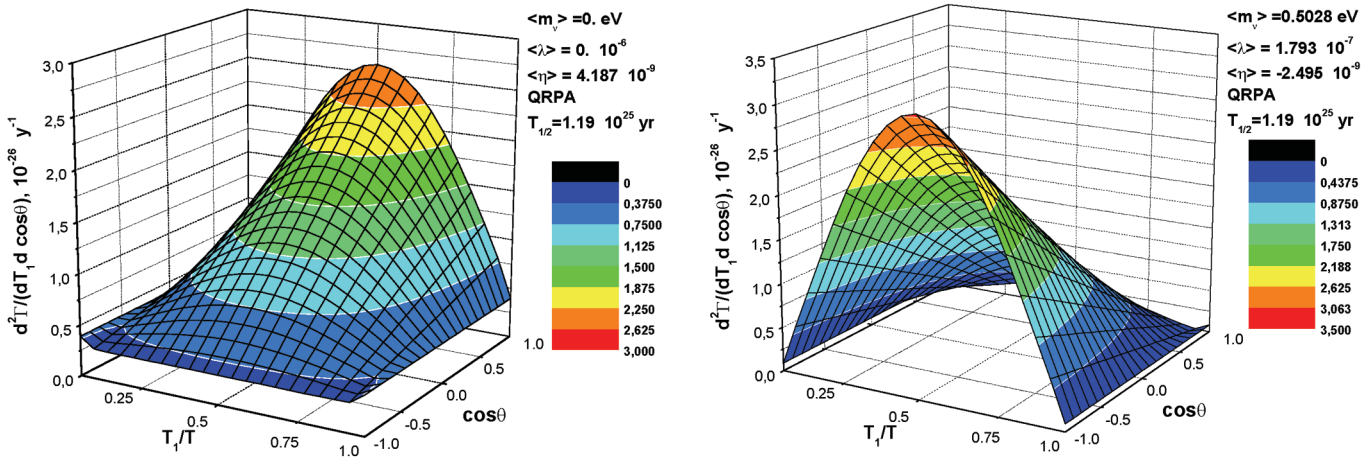

FIG. 4 (color). Calculated spectral-angular distribution for the $\langle\eta\rangle^2$-term for $0\nu\beta\beta$ decay of ^{76}Ge (left), and for the values $\langle m_\nu\rangle = 0.503$ eV, $\langle\lambda\rangle = 1.793 \cdot 10^{-7}$, $\langle\eta\rangle = -2.495 \cdot 10^{-9}$ (right). (QRPA from [28]).

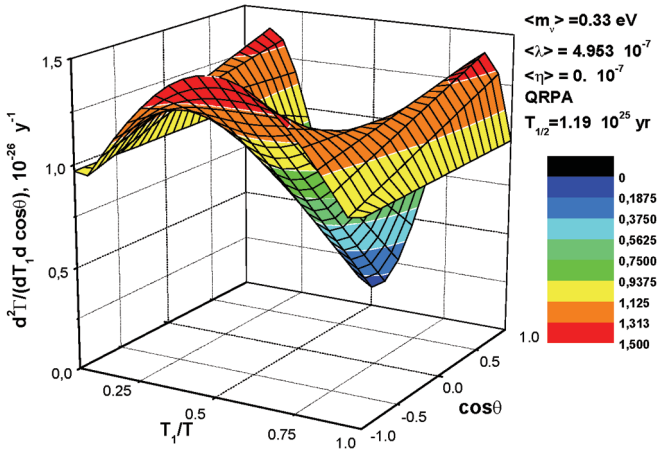

FIG. 5 (color). Calculated spectral-angular distribution for the parameters $\langle m_\nu \rangle = 0.33$ eV, $\langle \lambda \rangle = 4.953 \cdot 10^{-7}$, $\langle \eta \rangle = 0$, for $0\nu\beta\beta$ decay of ^{76}Ge (QRPA from [28]).

be emitted in opposite directions with energies equalling to half of the total kinetic energy or in the same directions with energies 15%/85% of the total kinetic energy. This shows that the shapes of the angular correlations can vary considerably within the 3σ-allowed range of parameters fixed by experiment.

We considered also other models of QRPA. Taking into account only the mass term from Eq. (21), the kinematical factor G_1 Eq. (27) and recent results for matrix elements published in [35,36] for different expansions of the QRPA nuclear model we calculated the effective neutrino mass, again starting from the experimental half-life $T^{0\nu}_{1/2} = 1.19 \cdot 10^{25}$ y [5,6]. The values of the matrix elements $M^2_{GT}(1 - \chi_F)^2$ for pnQRPA, pnRQRPA, full-QRPA and SQRPA, calculated with large single-particle basis (l) and small single-particle basis (s) are presented in the first row of Table II (see [35]). The numbers in the second row are the calculated effective neutrino masses in eV, calculated here with these matrix elements and the experimental half-life [5,6]. The spectral-angular distributions for these parameters of mass are very similar to the distributions presented in Figs. 3—left and 4—(right).

TABLE II. Nuclear matrix elements of the neutrinoless double-beta decay of ^{76}Ge in different variations of QRPA (see [35]) and upper limits for the neutrino mass from ^{76}Ge. See text.

	(l)	(s)
pnQRPA	1.71	4.45
	0.826	0.317
pnRQRPA	1.87	3.74
	0.755	0.384
Full-QRPA	2.40	3.68
	0.588	0.384
SQRPA	3.21	3.82
	0.440	0.370

C. Spectral-angular distribution for the shell model (SM)

The shell model has, as mentioned, in contrast to QRPA, general problems to describe the large configuration space of a heavy nucleus such as of ^{76}Ge (see [27]) and this is particularly true for these early calculations, which we use here as didactical example. According to Table I in the frame of the shell model approach from [33] the matrix element for the P-wave effect has the opposite sign in comparison to the QRPA, and the recoil matrix element is now zero. In the spectral-angular distribution Eq. (30) the $\langle\lambda\rangle\langle\eta\rangle$ -term has the opposite sign now. According to the values of Table I we find for the shell model the constraints on the effective neutrino mass and on the two parameters of right-handed current shown in Fig. 6.

The following results for the effective neutrino mass and the right-handed parameters were obtained:

$$\begin{aligned} &\langle m_\nu \rangle = 0.355 \text{ eV}, \quad \langle \lambda \rangle = 0, \langle \eta \rangle = 0; \\ &\langle m_\nu \rangle = 0 \text{ eV}, \quad \langle \lambda \rangle = 6.789 \cdot 10^{-7}, \quad \langle \eta \rangle = 0; \\ &\langle m_\nu \rangle = 0 \text{ eV}, \quad \langle \lambda \rangle = 0, \quad \langle \eta \rangle = 1.004 \cdot 10^{-7}. \end{aligned} \tag{37}$$

According to expression (30) the spectral-angular distribution was calculated for these parameters and for the parameters $\langle m_\nu \rangle = 0.4224$ eV, $\langle \lambda \rangle = 1.89 \cdot 10^{-7}$, $\langle \eta \rangle = 0.611 \cdot 10^{-7}$, respectively. The results are presented in Figs. 7 and 8.

But, for example, for parameters $\langle m_\nu \rangle = 0.355$ eV, $\langle \lambda \rangle = 2.147 \cdot 10^{-7}$, $\langle \eta \rangle = 1.059 \cdot 10^{-7}$, also allowed by experiment (see Fig. 6), the angular distribution is isotropic (Fig. 9). The electrons can be emitted in different directions with half of total kinetic energy each.

D. Spectral-angular distribution for the VAMPIR approach

The constraints on the effective mass of the neutrino and on the two parameters of right-handed currents for the VAMPIR approach are presented in Fig. 10.

The phenomenological analysis yields the following values for the effective mass of the neutrino and for the two right-handed parameters:

$$\begin{aligned} &\langle m_\nu \rangle = 0.256 \text{ eV}, \quad \langle \lambda \rangle = 0, \quad \langle \eta \rangle = 0 \\ &\langle m_\nu \rangle = 0 \text{ eV}, \quad \langle \lambda \rangle = 6.102 \cdot 10^{-7}, \quad \langle \eta \rangle = 0; \\ &\langle m_\nu \rangle = 0 \text{ eV}, \quad \langle \lambda \rangle = 0, \quad \langle \eta \rangle = 5.945 \cdot 10^{-9}. \end{aligned} \tag{38}$$

The spectral-angular distributions for these sets of parameters and for the set of parameters $\langle m_\nu \rangle = 0.302$ eV, $\langle \lambda \rangle = 1.208 \cdot 10^{-7}$, $\langle \eta \rangle = -3.533 \cdot 10^{-9}$ (Fig. 11) are very similar to the distributions for QRPA.

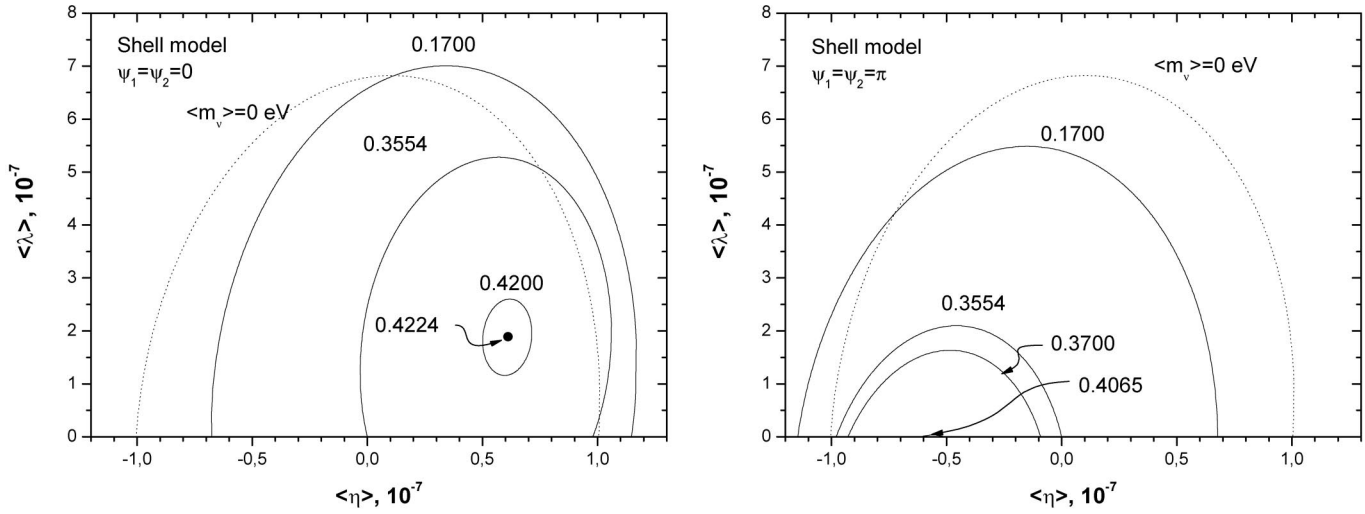

FIG. 6. Allowed parameters for $\langle m_\nu \rangle$, $\langle \lambda \rangle$, $\langle \eta \rangle$ from the measured half-life of $0\nu\beta\beta$ decay of ^{76}Ge [5] with matrix elements from the shell model from Table I.

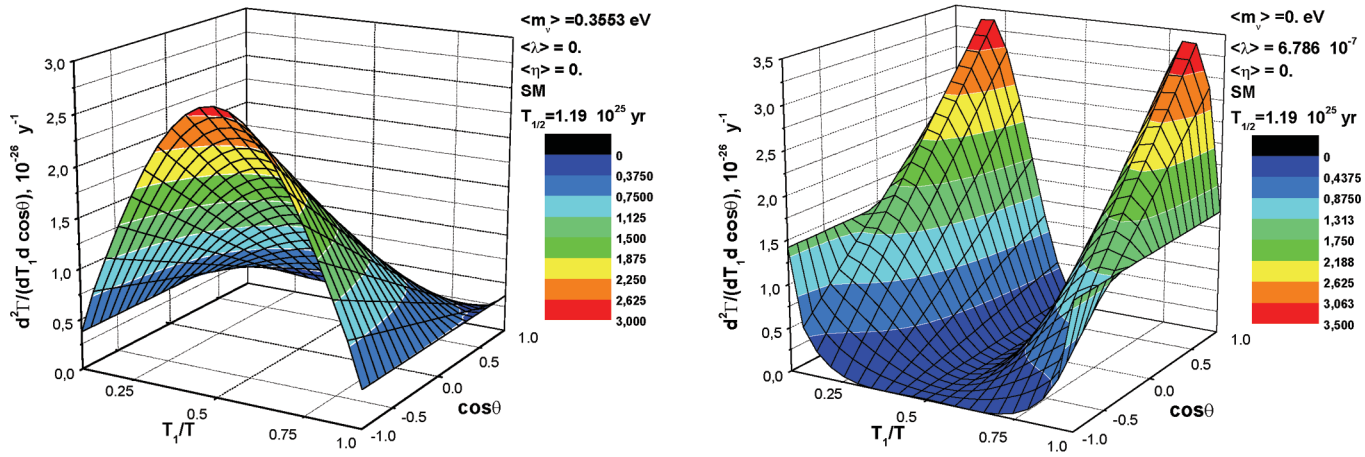

FIG. 7 (color). Calculated spectral-angular distribution for the neutrino mass term for $0\nu\beta\beta$ decay of ^{76}Ge (left) and for the $\langle \lambda \rangle^2$-term (right) (for matrix elements from SM [33]).

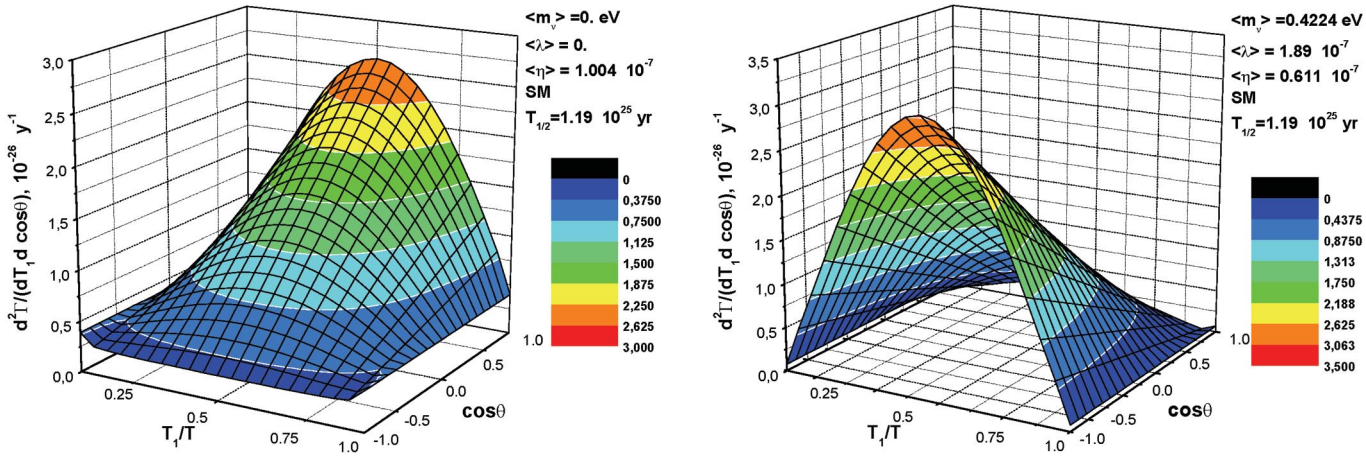

FIG. 8 (color). Calculated spectral-angular distribution for the $\langle \eta \rangle^2$ -term for $0\nu\beta\beta$ decay of ^{76}Ge (left) and for the parameter set $\langle m_\nu \rangle = 0.4224$ eV, $\langle \lambda \rangle = 1.89 \cdot 10^{-7}$, $\langle \eta \rangle = 0.611 \cdot 10^{-7}$ (right) (with matrix elements from shell model [33]).

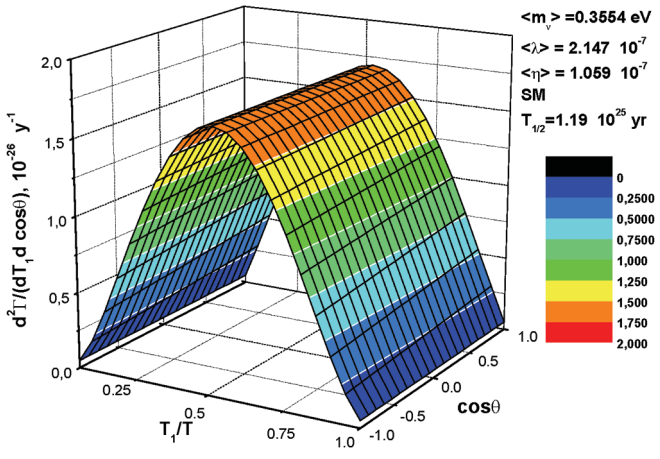

FIG. 9 (color). Calculated spectral-angular distribution in $0\nu\beta\beta$-decay of ^{76}Ge for $\langle m_\nu\rangle = 0.3554$ eV, $\langle\lambda\rangle = 2.147 \cdot 10^{-7}$, $\langle\eta\rangle = 1.059 \cdot 10^{-7}$ (matrix elements from shell model [33], see Table I).

The comparison of the three models shows that the sensitivity of the angular correlations of the electrons emitted in $0\nu\beta\beta$ decay on the nuclear models seems to be rather moderate.

III. MONTE-CARLO SIMULATIONS OF TRACKS AND SIZES OF $\beta\beta$ AND GAMMA EVENTS IN THE GE DETECTOR

A. General

The $\beta\beta$ decay, and photon interactions in a Ge detector including photoelectric absorption, Compton scattering and pair-production result in fast electrons that lose energy via Compton interactions in the germanium crystal and via bremstrahlung. The produced free electrons and holes drift in opposite directions along the electric field created by the reverse bias voltage applied to a p-type Ge detector. This charge separation and drift induces an image current on the electrodes. When these charge carriers reach the electrodes, they are collected and no longer contribute to the current. The total energy deposited is proportional to the charge obtained by integrating this current over time. The shape of the induced current pulse depends on the electric field inside the detector, the position and *size* (more precisely the spatial distribution of the energy depositions) and the effects of external electronics.

Calculations were made for 2ν and $0\nu\beta\beta$ events from the decay of ^{76}Ge, and for photon events from nuclear transitions 2614 keV, 2204 keV and 1620 keV, for the sizes of the full energy lines (FE) and for the size of single- and double-escape (SE and DE) events for the lines 2614 keV and 2204 keV, respectively, and for the size of events in the energy range 2035–2043 keV ($Q_{\beta\beta} = 2039$ keV [37–40]) resulting by Compton scattering from transitions 2614 keV and 2204 keV, for one of the detectors of the HEIDELBERG-MOSCOW experiment which is a coaxial p-type HP Ge detector of about 2.7 kg active mass.

The γ-events were started from an imaginary source *outside* the detector. The geometry of the enriched detector (see Fig. 12) was taken from files for the calculations of all known background components for the HEIDELBERG-MOSCOW experiment [25].

While the location and energy depositions for photon events are determined by a standard Monte-Carlo photon routine (GEANT 4 [41]), both modes of $\beta\beta$ decay could not be simulated in the GEANT 4 code directly. For the simulation the following model has been used: the two electrons were started at a defined point *in* the detector, the energy, and the angle between the directions of their impulses were defined according to the *spectral-angular distributions for the neutrino-accompanied and the neutrinoless modes of $\beta\beta$ decay*, calculated in the previous section. Then the history of the events was determined by the Monte-Carlo procedure.

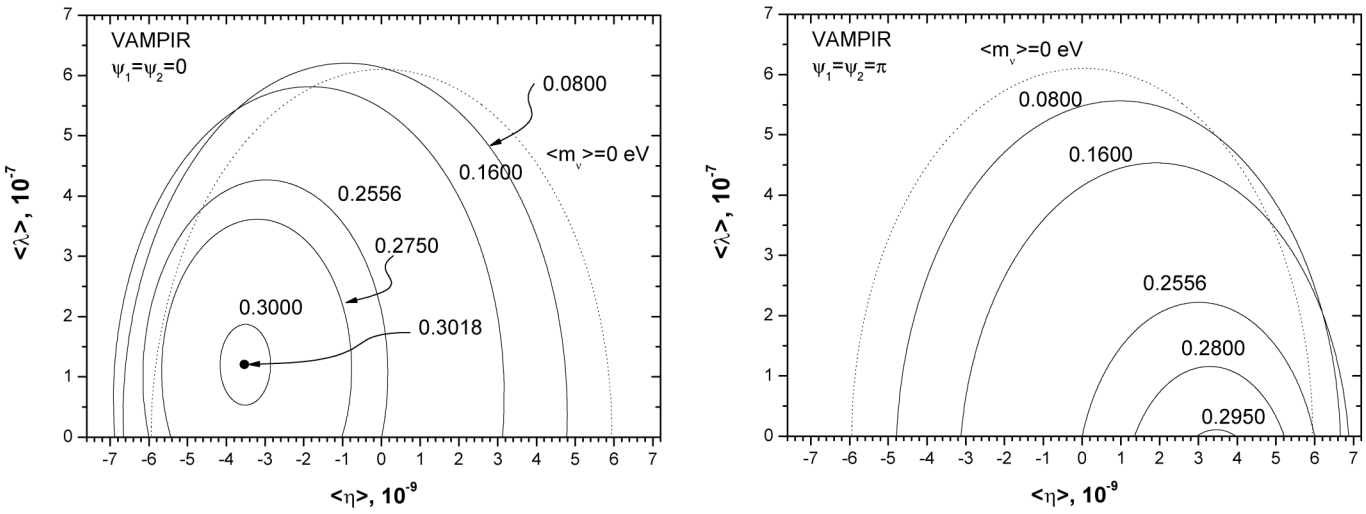

FIG. 10. Allowed parameters $\langle m_\nu\rangle$, $\langle\lambda\rangle$, $\langle\eta\rangle$ from ^{76}Ge $0\nu\beta\beta$ decay [5,6] according to analysis with VAMPIR from Table I.

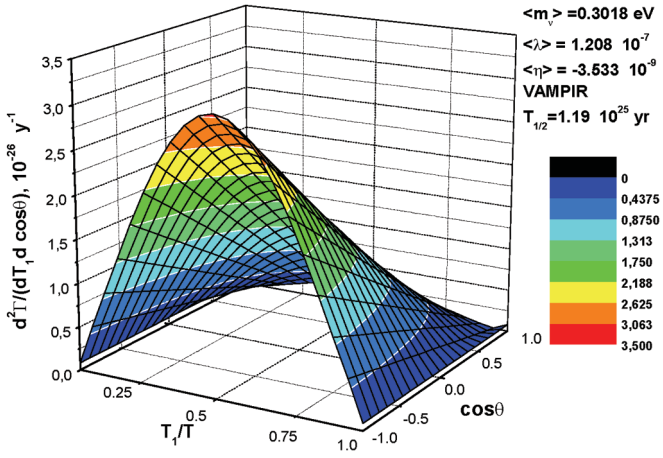

FIG. 11 (color). Calculated spectral-angular distribution for $0\nu\beta\beta$ decay of ^{76}Ge and $\langle m_\nu\rangle = 0.3018$ eV, $\langle\lambda\rangle = 1.208\cdot10^{-7}$, $\langle\eta\rangle = -3.533\cdot10^{-9}$, with the VAMPIR approaches.

B. Calculation of $2\nu\beta\beta$ and $0\nu\beta\beta$ Event Histories

For the calculation of the neutrino-accompanied mode of $\beta\beta$ decay we choose two cases for the total kinetic energy release from the electron spectrum: a point with energy 700 keV (near maximum of the spectrum at 673 keV) and the point with 2000 keV (near $Q_{\beta\beta}$). The energy distribution and angle between the two electrons were chosen according to the results shown in Fig. 1 (approximately 0.1T for one electron and 0.9T for the other, the angle between the directions of their impulses was chosen to be 180°).

For the calculation of the $0\nu\beta\beta$ events the three cases in Eq. (34) were considered, according to the main features of the calculated angular correlations:

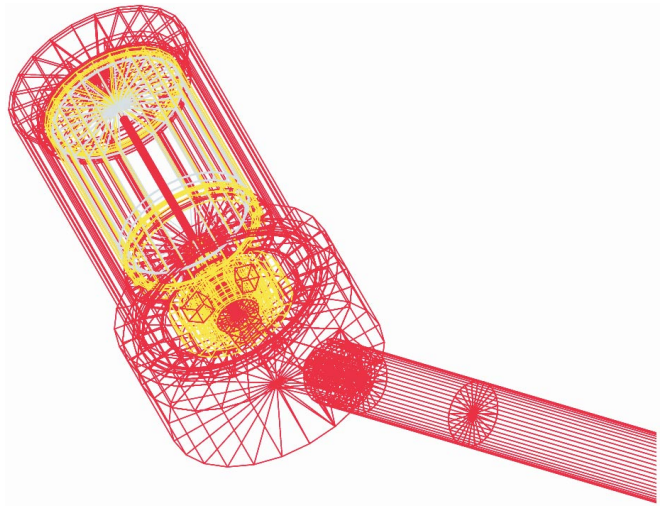

FIG. 12 (color). The geometry of one of the five enriched Ge detectors of the HEIDELBERG-MOSCOW double-beta experiment (from [25]).

(1) At first two electrons with energy 1020 keV each, were started at a given point in the detector. The angle between the directions of their impulses was 180° (only the neutrino mass part for the spectral-angular distribution was taken into account, see Figs. 3—left, 7—left).
(2) Then the calculations were made for the case when the $\langle\lambda\rangle$ parameter is nonzero. The directions of the electrons were the same and the energy distribution according to the results shown in Figs. 3—right and 7—right (approximately 0.15 T for one electron and 0.85 T for the other).
(3) For the case when only the η term is nonzero (Figs. 4—left and 8—left), the electrons were assumed to be emitted to the same direction with half of the total kinetic energy each.

Then the time history of subsequent scattering or absorption events were calculated. The values of the energy depositions and coordinates of each interaction in the decay processes were written in data files. For the neutrino-accompanied mode in total 99606 events were calculated with full energy of 700 keV, and 95818 events for 2000 keV.

For the $0\nu\beta\beta$ mode, in the first case, when only the mass term is taken into account, in total 96820 $\beta\beta$ events were calculated. For the second and third cases of spectral-angular distributions in total 95902 and 97768 events were considered, respectively. Some examples of calculated tracks of $0\nu\beta\beta$ events in the germanium detector are presented in Fig. 13. The places of the energy depositions in germanium are indicated as circles. The sizes and colors of these circles indicate the amount of energy released at these points. Green lines denote γ-events (bremsstrahlung) in case of $\beta\beta$ decay, annihilation gammas in case of absorption of a γ by pair creation, all other events are electron(positron)-electron scattering.

Figure 14 shows the calculated energy spectrum of $0\nu\beta\beta$ decay for the first case of $\beta\beta$-events (mass-term nonzero, right-handed current parameters zero). The sum energy of the two electrons is shown on the x-axis. Most events lie in the sharp main peak at $Q_{\beta\beta}$ (2039 keV). The broad peak around 1850 keV corresponds to events with bremstrahlung emission. The shoulder around 1020 keV is formed when the energy of only one electron is deposited in the detector (when the decay process happened near the edge of the detector). In total 94% of the $0\nu\beta\beta$ events are seen in the peak of $0\nu\beta\beta$.

C. Calculation of Photon Events

For the calculations of photon events the imaginary source of the photons with energy 2614 keV/2204 keV/1620 keV was put on the top part of the detector at a radius of 20 mm. The distance between top part of detector and source of the photons was 100 mm (the thickness of the lead collimator). The diameter of the hole in the collimator

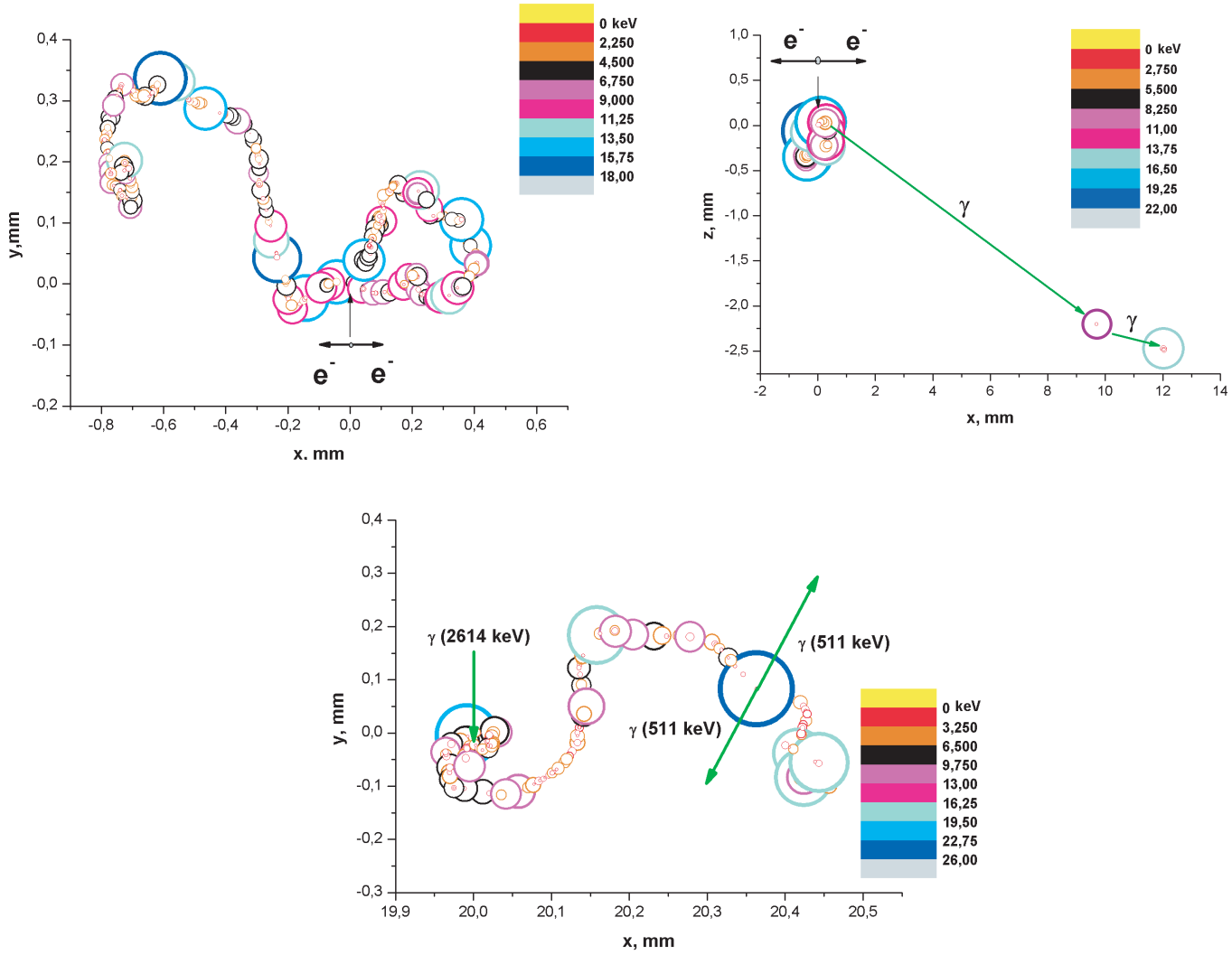

FIG. 13 (color). Upper part: Typical calculated $0\nu\beta\beta$ decay event without photon emission (bremstrahlung) (left), and with photon emission (bremstrahlung) (right). Low part: Calculated photon event (the energy of the initial photon is 2614 keV) for the double-escape case (leading to a line in the detector at 1592 keV). For further explanation see text.

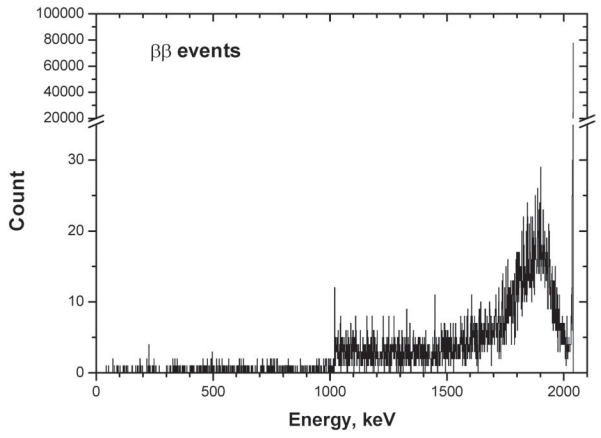

FIG. 14. The calculated energy spectrum of $0\nu\beta\beta$ decay of ^{76}Ge, as seen in an enriched ^{76}Ge detector. The sum of the energies of the emitted electrons is shown on the x-axis.

was 2 mm. For our investigations only events were considered which passed through the collimator without scattering in the lead. For these photon events the statistics was the following: 299365 photon events with initial energy 2614 keV, 298427 events with energy 2204 keV and 104193 events with 1620 keV were calculated. Figure 13 shows an example of a photon event in the detector. Figures 15 and 16 show the spectrum seen in the detector (according to the Monte-Carlo simulation) from the 2614 keV γ-transition. Besides the full energy (FE) peak at 2614 keV the single escape (SE) and double-escape (DE) peaks occur, resulting from absorption of the 2614 keV γ-quant by e^+e^- pair creation and subsequent annihilation of the positron with an electron and emission of two 511 keV γ-quanta, of which one (SE) or both (DE) escape from the detector (see, e.g. [6,42–44]). The figures show also the contribution of Compton scattered events of

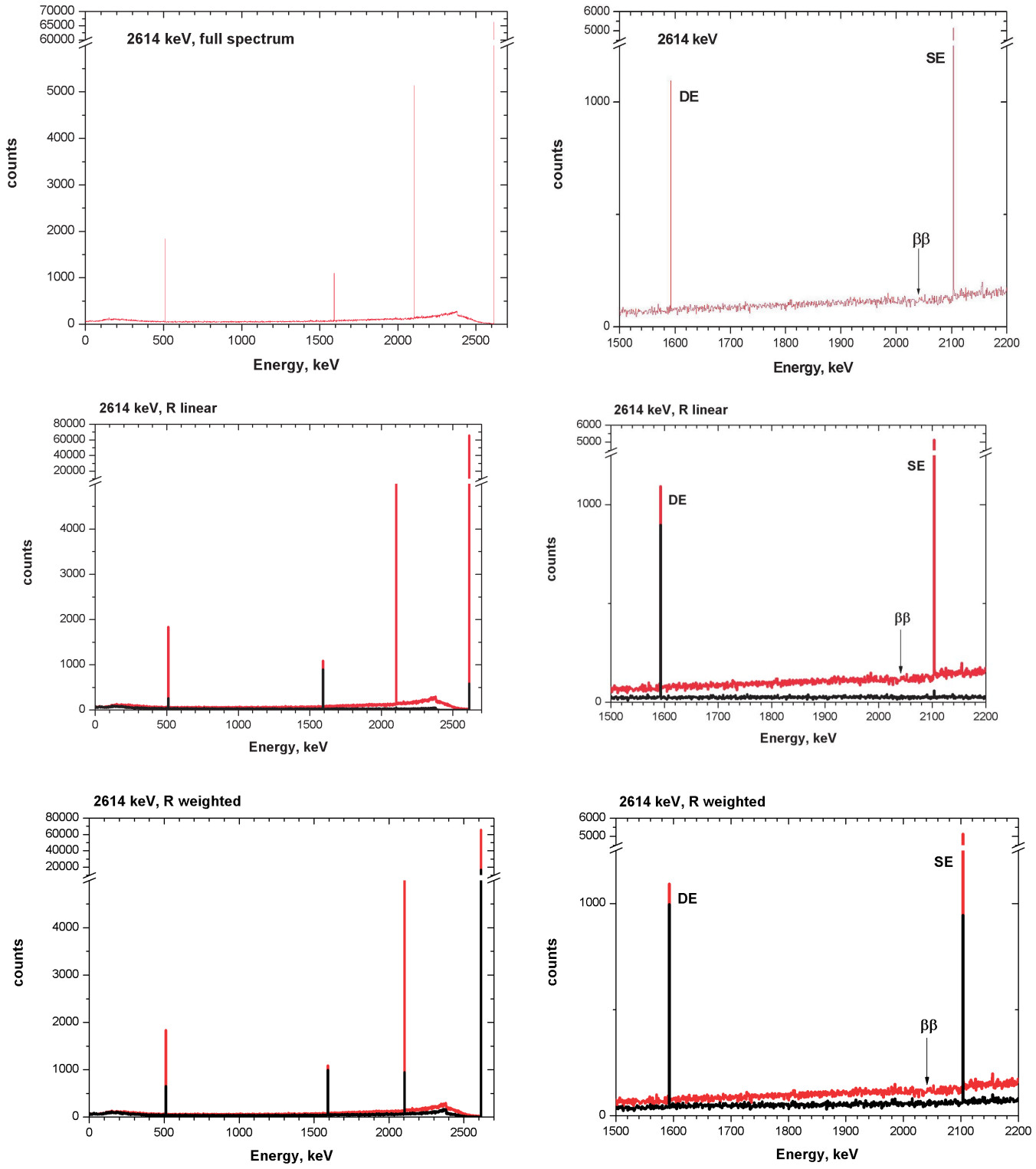

FIG. 15 (color). Simulation of the spectrum seen in the detector for the 2614 keV γ-transition: Upper part: the full spectrum (left) and the zoomed part for the 1500–2200 keV region (right). The middle and lower parts show *in addition* to the (red) full spectra also the (black) spectra consisting only of events with diameter ≤ 2 mm (for the linear and weighted sizes, respectively) (see Sec. III D).

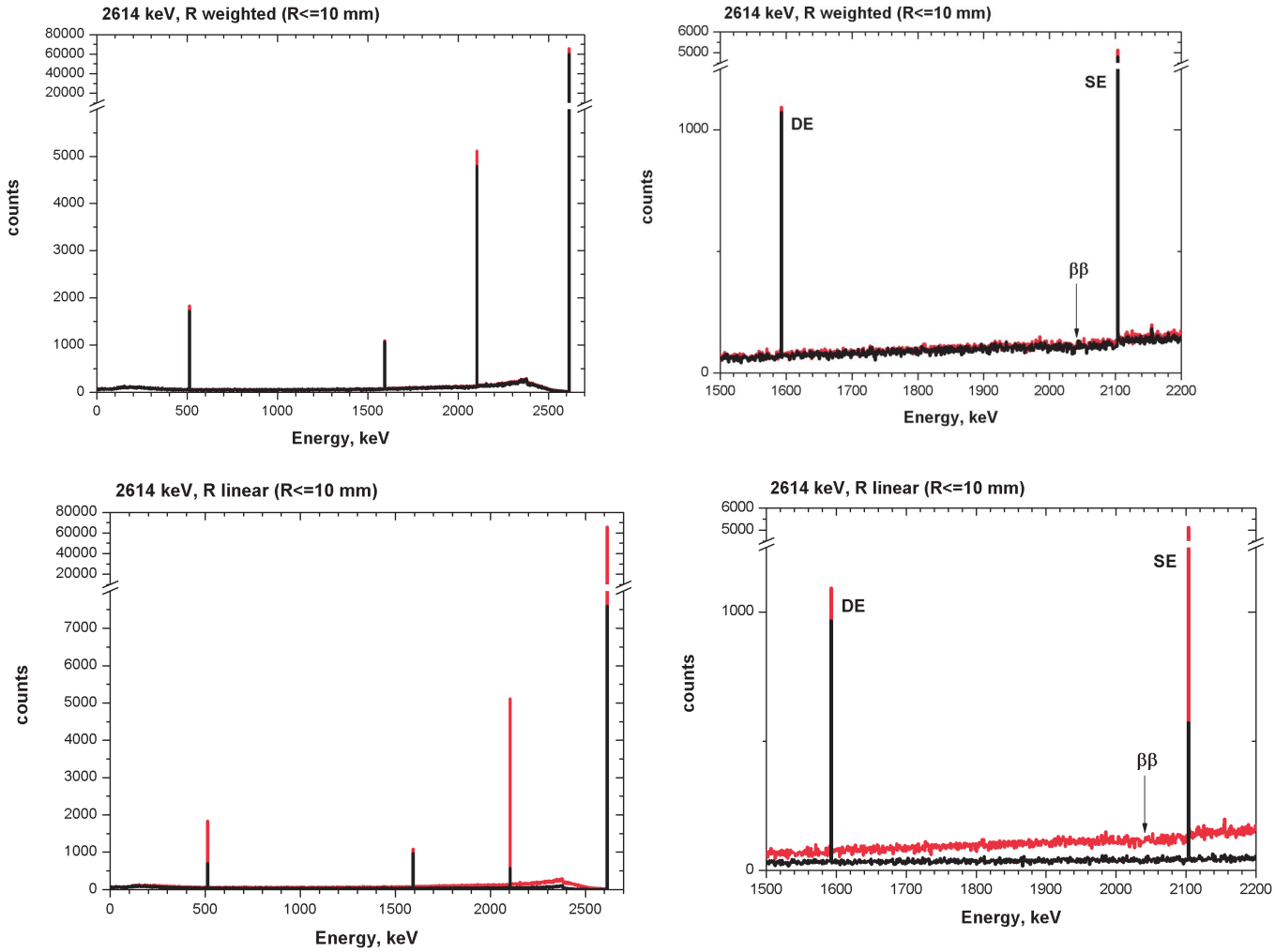

FIG. 16 (color). Simulation of the spectrum seen in the detector for the 2614 keV γ-transition: the full spectrum (left) and the zoomed part for the 1500–2200 keV region (right). The upper and lower parts show *in addition* to the (red) full spectra also the (black) spectra consisting only of events with diameter $\leq$ 10 mm (for the linear and weighted sizes, respectively) (see Sec. III D).

different sizes (see Sec. III D) to the spectrum (which occur as continuous background near $Q_{\beta\beta}$ in the double-beta decay measurement).

D. Sizes of Events

The sizes of individual events such as shown in Fig. 13 were defined according to two different methods. The *linear size* was calculated as the maximum distance between places of energy depositions without paying attention to the values of latter:

$$R_l = \max[\sqrt{(x_i - x_j)^2 + (y_i - y_j)^2 + (z_i - z_j)^2}]. \quad (39)$$

In the definition of the "weighted" size the values of energy deposited in each point were taken into account:

$$R_W = \frac{\sum_{i,j} \epsilon_i \epsilon_j \sqrt{(x_i - x_j)^2 + (y_i - y_j)^2 + (z_i - z_j)^2}}{\epsilon_{\text{total}}^2}, \quad (40)$$

where ϵ_{total} is the full energy, deposited for this event in the detector. While naturally in the first case in a range of diameter R, 100% of the released energy is contained, in the weighted case a volume with diameter R_w contains typically about 60% of the total released energy.

In the analysis of sizes of events the cases 1–3 of Sec. III B were considered for $0\nu\beta\beta$ decay (energies in the detector are for ~94% of the events equal to $Q_{\beta\beta}$). For $2\nu\beta\beta$ decay two energies were considered (700 and 2000 keV). For photon events four energy regions were considered: Compton scattering in the energy region around $Q_{\beta\beta}$ (2035–2043 keV), double-escape (DE) region, single escape (SE) region and the main line (full energy peak) (Figs. 15 and 16).

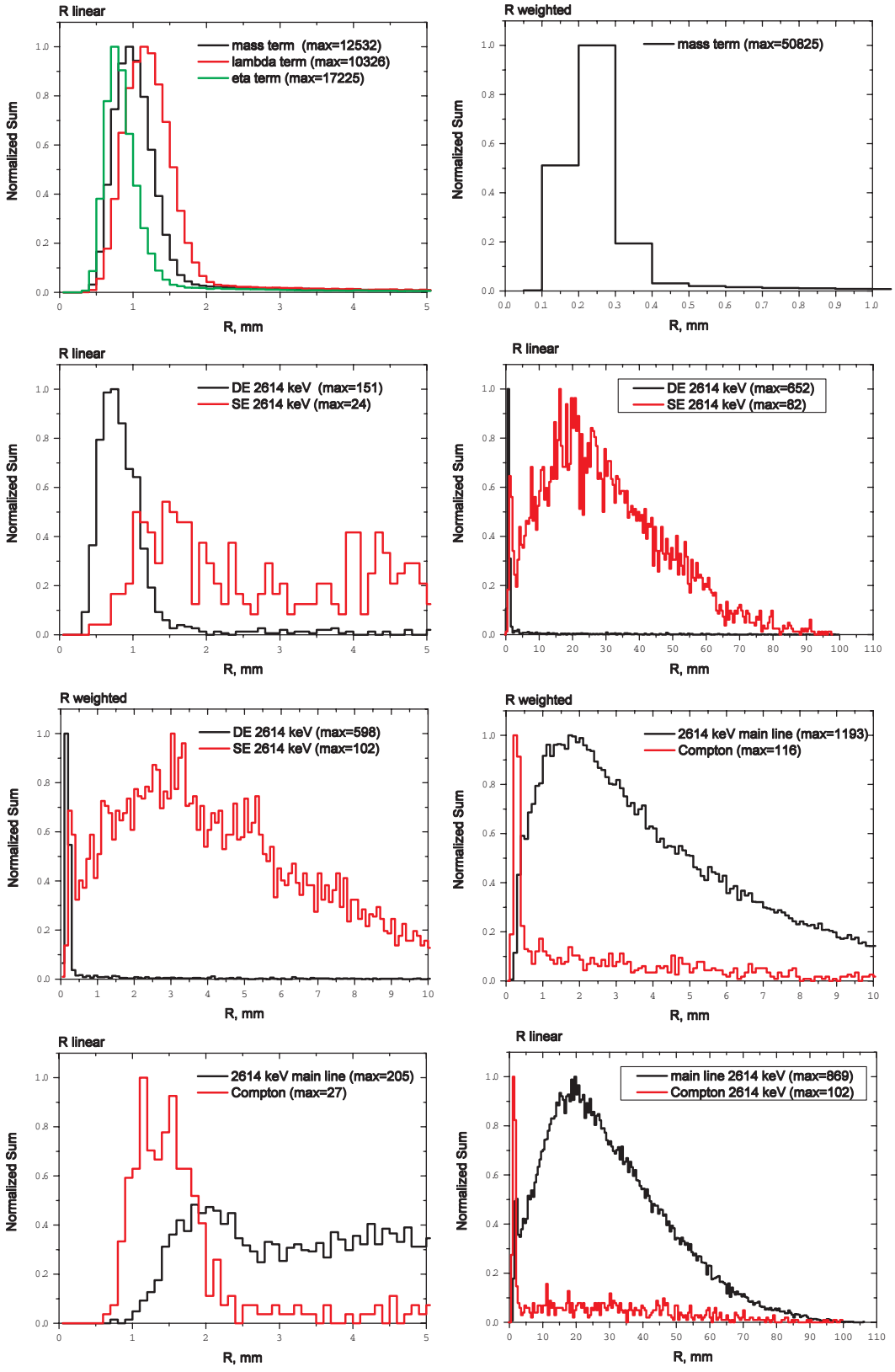

FIG. 17 (color). Distribution of sizes (linear and weighted) in a Ge detector of various types of $0\nu\beta\beta$ events, and of the γ-line at 2614 keV, and its single and double-escape lines at 2103 keV and 1592 keV, respectively, and of the Compton events produced by this γ-transition in the range around $Q_{\beta\beta}$ (2035–2043 keV), according to Monte Carlo simulations of these events taking into account the angular correlations between the emitted electrons in $0\nu\beta\beta$ decay.

In our calculations for these energy regions the following statistics was obtained:

(a) For 2614 keV: for Compton-scattering in the energy range 2035-2043 keV - 921 events, for the SE line—5382 events, for the DE line—1249 events, for the main line—66024 events.

(b) For 2204 keV: for Compton-scattering in the energy range 2035–2043 keV - 1167 events, for the SE line—3389 events, for the DE line—816 events, for the main line—72466 events.

c) For 1620 keV: for the main (FE) line—28651 events.

The results of the calculations for "linear" and "weighted" event sizes are presented in a differential way in Fig. 17 and in integral way in Figs. 18 and 19. On the ordinate axis of Figs. 18 and 19 the normalized sum is presented. In Fig. 17 maximum intensities are normalized to 1 (except for figures (c)(g), which are just part of figures (d)(h)). It is clear that ~95% of $0\nu\beta\beta$ events lie within a distance of 2 mm for calculations of the 'weighted' size (Eq. (40)) and ~85% events for calculations of the linear events size (Eq. (39)). For the Compton-scattering region (2035–2043 keV) for 'weighted' and 'linear' sizes definition only ~50% and ~30% of events, respectively, lie within this distance. The Compton events in the range $R_l < 1$ mm are only a few percent, while still ~45% of the $0\nu\beta\beta$ events will occur within this range. The parts of the SE and the main line within 2 mm are only ~20% and ~25% for the weighted sizes and a few percent for the linear sizes. The maxima of the distributions of sizes are around 20–30 mm (linear size) for the full energy line and the single escape line of the 2614 keV transition. These latter two types of events are mainly MSE (see Figs. 15 and 16). The $\beta\beta$ events are mainly SSE and we can clearly distinguish them by size. The situation with DE gamma events is different. Since the DE events are mainly SSE (see Figs. 15 and 16), their size is very similar to the $0\nu\beta\beta$ events, but systematically slightly *smaller* in size. About 80/75% (weighted/linear) of the DE events are lying within a distance of 2 mm.

Also the $2\nu\beta\beta$ events at 2000 keV are very close to the $0\nu\beta\beta$ events, while the $2\nu\beta\beta$ events at 700 keV—around the maximum of the 2ν continuous spectrum—have much smaller size. For the photon events of the 2204 keV γ-transition and the 1620 keV γ-transition the situation is similar to that of the 2614 keV transition.

Then we compared $0\nu\beta\beta$ events sizes for our three cases (see Eq. (34) and Sec. III B) of spectral-angular distribution (Fig. 19). It is obvious from Fig. 19 that it *would be extremely difficult* with the typical spatial resolution of a large Ge detector of the order of mm (linear), to distinguish the different particle physics cases by size of the corresponding events. This has the advantage that for the parameters in the experimentally allowed 3σ range the sizes of the $0\nu\beta\beta$ events will be *practically* the same (compare also the curves for the mass-term and for $\langle m_\nu \rangle = 0.33$ eV in Fig. 19).

On the other hand Fig. 17 shows, that to a large extent it should be possible to distinguish Compton events in the energy range around $Q_{\beta\beta}$, and $0\nu\beta\beta$ -events by event size. Since the DE events are mainly similar in size to the $\beta\beta$-events, this suggests the possibility to use the DE events of the 2614 keV line from ^{228}Th for some pulse shape 'calibration' of the detector (see [5,6]). Of course a DE γ-line *at* $Q_{\beta\beta}$ could *hardly* be separated from $0\nu\beta\beta$ events. However, such line should always have a corresponding *much* stronger full energy line at energy

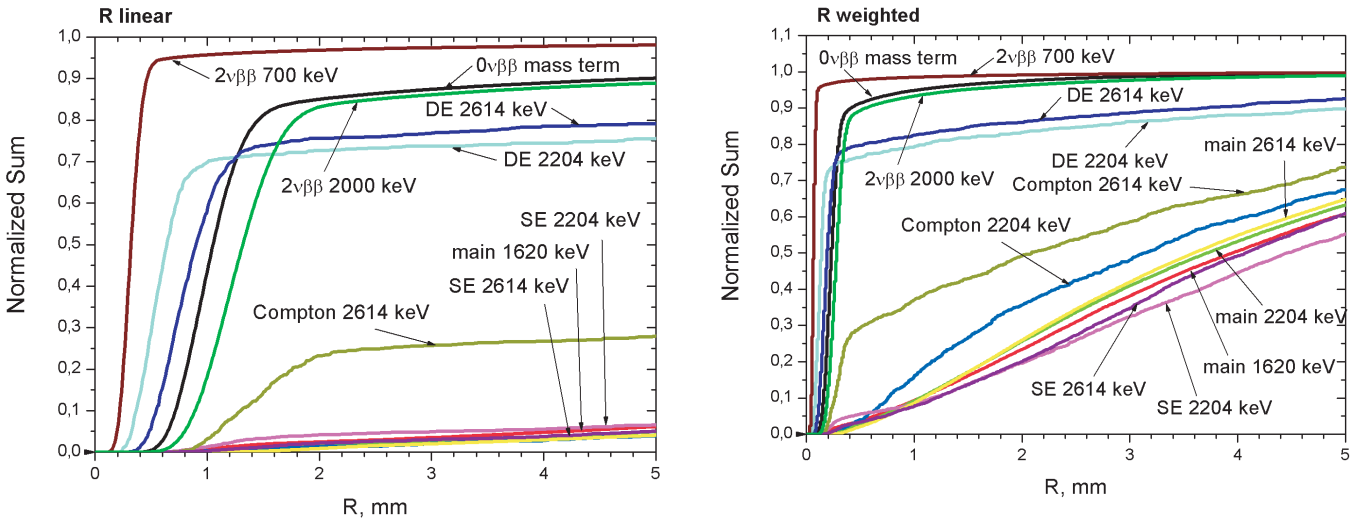

FIG. 18 (color). Calculated events sizes of $\beta\beta$ events (only mass term considered), and of γ-transitions 2614, 2204 and 1620 keV. For the first two in addition to the main line (full energy peak), also shown are the sizes of the double-escape (DE) and single escape (SE) peaks, and of Compton events in the range 2035–2043 keV.

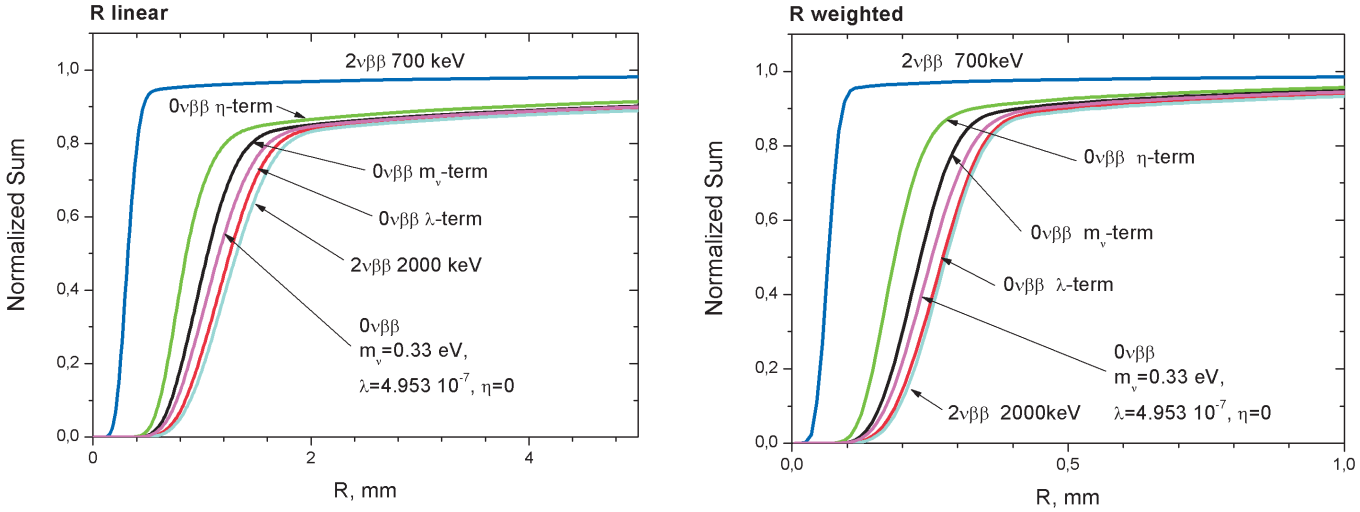

FIG. 19 (color). Calculated event sizes of $0\nu\beta\beta$ events for the $\langle m_\nu\rangle$, $\langle\eta\rangle$, $\langle\lambda\rangle$ parameter sets of Eq. (34) and for $\langle m_\nu\rangle = 0.33$, $\langle\lambda\rangle = 4.95 \times 10^{-7}$, $\langle\eta\rangle = 0$.

$Q_{\beta\beta} + 1022$ keV (see Figs. 15 and 16 as examples). Also some differentiation of the main part of $2\nu\beta\beta$ events from gamma events might be possible (Figs. 18 and 19).

IV. SUMMARY AND CONCLUSIONS

A first systematic study has been performed of the sizes of double beta and γ-events in a Ge detector, which finally largely determine, together with the location of the events in the detector, the shapes of the pulses seen in the detector. For this purpose, time history and tracks of individual events have been calculated by a Monte Carlo procedure based on GEANT 4, for $0\nu\beta\beta$ and $2\nu\beta\beta$ decay, including the main effects of the simulated angular correlations between the two emitted electrons, and for different kinds of photon interactions which contribute to the background in measured $0\nu\beta\beta$ and $2\nu\beta\beta$ spectra. The $\beta\beta$ angular correlations which depend on the effective neutrino mass and the right-handed coupling parameters η and λ, have been calculated for this purpose for the first time starting from the experimental $\beta\beta$ half-lives and with realistic matrix elements. It is found that the ''sizes'' of the events (partial volumes in the detector in which the energy is released) *show strong differences* for $0\nu\beta\beta$ and $2\nu\beta\beta$ events at $\sim$2000 keV on one side, and most of the Compton scattered gamma events in the energy range of $Q_{\beta\beta}$ on the other side. Further, the events from the full energy γ-lines and the corresponding single escape peaks *differ strongly* in size from the $0\nu\beta\beta$ events. Therefore, $0\nu\beta\beta$ events in a ^{76}Ge detector should be selectable by rejecting large size (high multiplicity) strong γ events. The events in the DE peaks of the γ-lines come—in size—close to the behavior of $0\nu\beta\beta$ events. They were therefore of interest for pulse shape ''calibration'' of a $0\nu\beta\beta$ decay detector [5,6].

The differences in sizes of $0\nu\beta\beta$ events for different choice of particle physics parameters $\langle m_\nu\rangle$, $\langle\lambda\rangle$, $\langle\eta\rangle$ are too small to be realized with the position resolution of a large Ge detector. This has the advantage, that the deduced possibility to distinguish $\beta\beta$ events from γ-events is essentially independent of the particle physics parameters of the $0\nu\beta\beta$ process.

Finally let us have a look into the potential of *future* $0\nu\beta\beta$ experiments with respect to the determination of the particle physics parameters $\langle m_\nu\rangle$, $\langle\lambda\rangle$, $\langle\eta\rangle$.

It has been mentioned in the Introduction that *none* of the future double-beta experiments like EXO, (Super-) NEMO or CUORE etc., will ever be able to identify *tracks* of neutrinoless double-beta decay. But *even if* in some kind of future experiment the tracks *could* be clearly differentiated, then according to Figs. 3–5, 7–9, and 11 there would be *never a chance* to get information about the particle physics parameters dominating the $0\nu\beta\beta$ process, particularly in a low-statistics experiment.

This means that *no future single* double-beta $0^+ \rightarrow 0^+$ $\beta^-\beta^-$ experiment will be able to obtain more information then a ^{76}Ge experiment. No confirmation by *another* $0^+ \rightarrow 0^+$ $\beta^-\beta^-$ experiment would yield any new additional information. It has been pointed out earlier [45] that *also several* simultaneous experiments looking for $\beta^-\beta^-$ *decay* cannot yield more information. E.g., if to the result of the ^{76}Ge (HEIDELBERG-MOSCOW) experiment the result of a high-sensitivity ^{136}Xe experiment would be added, *no fundamental new* information would be obtained (see Fig. 3(a) in [45]). The *only realistic way* we see to obtain information on the individual mass and right-handed weak current parameters $\langle m_\nu\rangle$, $\langle\lambda\rangle$, $\langle\eta\rangle$, is [45] from a simultaneous analysis of a high-sensitive $\beta^-\beta^-$ experiment (which has *observed* $0\nu\beta\beta$ decay, as ^{76}Ge), *and* a suitable *very high-sensitive mixed-mode experiment* looking for

$0\nu\beta^+$EC decay (e.g. ^{124}Xe) on a half-life level of 10^{27} years.

Another theoretical possibility is to look for the $0\nu\beta\beta$ half-life for the $0^+ \rightarrow 2^+$ transition, e.g. in ^{76}Ge, for which the mass mechanism vanishes in first order and the transition is driven mainly by the λ and η mechanism. Since the half-life to be expected [45,46] for these modes would lie, however, with $\sim 10^{30}$ and $\sim 5 \times 10^{32}$ years almost in the range of that of proton decay, such experiment may be only of academic interest.

ACKNOWLEDGMENTS

The authors acknowledge the invaluable support from DFG, and LNGS for this project. I. T. thanks the Max Planck Institut für Kernphysik for the hospitality, RFBR (Grant 02-02-04009) for support, and to V. Bednyakov for discussions.

[1] K. Grotz and H. V. Klapdor, *Die Schwache Wechselwirkung in Kern-, Teilchen- und Astrophysik* (Teubner, Stuttgart, 1989); *The Weak Interaction in Nuclear, Particle and Astrophysics* (IOP, Bristol, 1990); MIR, Moscow, (1992) and Shandong Science, Technology Press, Jinan (1998).

[2] J. Schechter and J. W. F. Valle, Phys. Rev. D **25**, 2951 (1982).

[3] R. N. Mohapatra, *Unification and Supersymmetry* (Springer, Heidelberg, 1986).

[4] H. V. Klapdor, Internal Report No. MPI-1987-V17, 1987 (unpublished).

[5] H. V. Klapdor-Kleingrothaus, I. V. Krivosheina, A. Dietz *et al.*, Phys. Lett. B **586**, 198 (2004); H. V. Klapdor-Kleingrothaus, I. V. Krivosheina, and I. V. Titkova, Phys. Lett. B **632**, 623 (2006).

[6] H. V. Klapdor-Kleingrothaus, A. Dietz, I. V. Krivosheina *et al.*, Nucl. Instrum. Methods Phys. Res., A **522**, 371 (2004).

[7] H. V. Klapdor-Kleingrothaus *et al.*, Mod. Phys. Lett. A **16**, 2409 (2001); Found. Phys. **32**, 1181 (2002).

[8] H. V. Klapdor-Kleingrothaus, in *Proc. of International Conf. "Neutrinos and Implications for Physics Beyond the Standard Model", Stony Brook, USA, 2002*, edited by R. Shrock (World Scientific, Singapore, 2003) p. 367; in *Proc. of Intern. Conf. "Beyond the Desert 2003", BEYOND03, Tegernsee, Germany, 2003, Springer, Heidelberg 2004*, edited by H. V. Klapdor-Kleingrothaus, p. 307.

[9] H. V. Klapdor-Kleingrothaus, in *Proc. of International Conf. "Neutrino 2004", Paris, France, 2004*; Nucl. Phys. B, Proc. Suppl. **143**, 229 (2005);

[10] H. V. Klapdor-Kleingrothaus, in *Proc. of International Workshop "Neutrino Oscillation—NOW 2004", Bari, Italy, 2004*, edited by G. Fogli *et al.*; Nucl. Phys. B, Proc. Suppl. **145**, 219 (2005);

[11] H. V. Klapdor-Kleingrothaus, in *Proc. of International Conf. "Neutrino Telescopes", Venezia, Italy, 2005*, edited by M. Baldo-Ceolin, p. 215.

[12] H. V. Klapdor-Kleingrothaus, Int. J. Mod. Phys. D **13**, 2107 (2004).

[13] J. Vuilleumier for the EXO collaboration, in *Proc. of International Workshop on the Identification of Dark Matter, Edinburg, Scotland, United Kingdom, 2004* (World Scientific, Singapore, 2005), p. 635.

[14] X. Sarazin *et al.*, in *Proc. of International Conf. "Neutrino 2004", Paris, France, 2004*; Nucl. Phys. B, Proc. Suppl. **143**, 221 (2005).

[15] E. Fiorini, in *Proc. of International Conf. "Neutrino 2004", Paris, France, 2004*; Nucl. Phys. B, Proc. Suppl. **143**, 225 (2005); C. Brofferio *et al.*, in *Proc. of International Conf. "Neutrino Telescopes", Venezia, Italy, 2005*, edited by M. Baldo-Ceolin, p. 239.

[16] J. Hellmig and H. V. Klapdor-Kleingrothaus, Nucl. Instrum. Methods Phys. Res., A **455**, 638 (2000).

[17] J. Hellmig, F. Petry, and H. V. Klapdor-Kleingrothaus, Patent DE19721323A.

[18] B. Majorovits and H. V. Klapdor-Kleingrothaus, Eur. Phys. J. A **6**, 463 (1999).

[19] M. Doi, T. Kotani, and E. Takasugi, Phys. Rev. C **37**, 2104 (1988).

[20] M. Doi, T. Kotani, and E. Takasugi, Prog. Theor. Phys. Suppl. **83**, 1 (1985).

[21] T. Tomoda, Rep. Prog. Phys. **54**, 53 (1991).

[22] K. Muto and H. V. Klapdor, *"Neutrinos", Graduate Texts in Contemporary Physics*, edited by H. V. Klapdor (Springer, Berlin, Germany, 1988) p. 183.

[23] M. Doi, T. Kotani, H. Nishiura, and E. Takasugi, Prog. Theor. Phys. **70**, 1353 (1983).

[24] M. Günther *et al.* (HEIDELBERG-MOSCOW Coll.), Phys. Rev. D **55**, 54 (1997).

[25] Ch. Dörr and H. V. Klapdor-Kleingrothaus, Nucl. Instrum. Methods Phys. Res., A **513**, 596 (2003).

[26] J. Suhonen and O. Civitarese, Phys. Rep. **300**, 123 (1998).

[27] H. V. Klapdor-Kleingrothaus, *60 Years of Double Beta Decay—From Nuclear Physics to Beyond the Standard Model* (World Scientific,, Singapore, 2001) p. 1281.

[28] K. Muto, E. Bender, and H. V. Klapdor, Z. Phys. A **334**, 177 (1989); K. Muto, E. Bender, and H. V. Klapdor, Z. Phys. A **334**, 187 (1989).

[29] W. A. Beg *et al.*, Phys. Rev. Lett. **38**, 1252 (1977).

[30] M. Doi, T. Kotani, H. Nishiura, K. Okuda, and E. Takasugi, Prog. Theor. Phys. **67**, 281 (1982).

[31] T. Tomoda *et al.*, Nucl. Phys. **A452**, 591 (1986).

[32] A. Staudt, K. Muto, and H. V. Klapdor-Kleingrothaus, Europhys. Lett. **13**, 31 (1990).

[33] W. C. Haxton and G. J. Stephenson, Prog. Part. Nucl. Phys.

12, 409 (1984).
[34] S. P. Rosen, Comments Nucl. Part. Phys. **18**, 31 (1988).
[35] S. Stoica and H. V. Klapdor-Kleingrothaus, Nucl. Phys. **A694**, 269 (2001).
[36] S. Stoica and H. V. Klapdor-Kleingrothaus, Phys. Rev. C **63**, 064304 (2001).
[37] G. Douysset *et al.*, Phys. Rev. Lett. **86**, 4259 (2001); I. Bergström *et al.*, in *Proc. of Intern. Conf. on Particle Physics Beyond the Standard Model, BEYOND'02, Oulu, Finland June 2002* (IOP, London, 2003), edited by H. V. Klapdor-Kleingrothaus, p. 197; I. Bergström*et al.*, in *Proc. of Intern. Conf., BEYOND 2003, Castle Ringberg, Germany, 2003, Springer, Heidelberg, 2003*, edited by H. V. Klapdor-Kleingrothaus, p. 397.
[38] J. G. Hykawy *et al.*, Phys. Rev. Lett. **67**, 1708 (1991).
[39] G. Audi and A. H. Wapstra, Nucl. Phys. **A595**, 409 (1995).
[40] R. J. Ellis *et al.*, Nucl. Phys. **A435**, 34 (1985).
[41] The GEANT4 collaboration, http://geant4.web.cern.ch/geant4/.
[42] B. Maier, Dissertation, Univ. of Heidelberg, 1995.
[43] G. F. Knoll, *Radiation Detection and Measurement*, (John Wiley & Sons, New York, 1989), 2nd ed.
[44] K. Siegbahn, *Alpha-, beta- and Gamma-Ray Spectroscopy* (North-Holland Publ. Company, Amsterdam, 1974), Vol. 1, 2, 4th printing.
[45] M. Hirsch, K. Muto, T. Oda, and H. V. Klapdor-Kleingrothaus, Z. Phys. A **347**, 151 (1994).
[46] T. Tomoda, Nucl. Phys. **A484**, 635 (1998).